

**PONTIFICIA UNIVERSIDAD
CATÓLICA DEL PERÚ**

Escuela de Posgrado



Mejora en la producción energética de un módulo fotovoltaico
bifacial vertical mediante la implementación de reflectores fijos
de aluminio

Trabajo de investigación para obtener el grado académico de
Maestro en Física Aplicada que presenta:

David Elias Nuñez Rishmawi

Asesor:

Jan Amaru Palomino Tofflinger

Co-asesor:

Guillermo Edmundo Baldwin Olguín

Lima, 2023

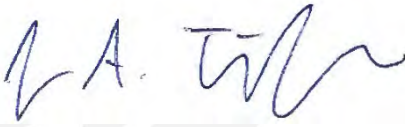
Informe de Similitud

Yo, **Jan Amaru Palomino Tofflinger**, docente de la Escuela de Posgrado de la Pontificia Universidad Católica del Perú, asesor de la tesis titulada “Mejora en la producción energética de un módulo fotovoltaico bifacial vertical mediante la implementación de reflectores fijos de aluminio” del autor **David Elías Núñez Rishmawi**, dejo constancia de lo siguiente:

- El mencionado documento tiene un índice de puntuación de similitud de 5%. Así lo consigna el reporte de similitud emitido por el software *Turnitin* el 29/11/2023.
- He revisado con detalle dicho reporte y la Tesis o Trabajo de Suficiencia Profesional, y no se advierte indicios de plagio.
- Las citas a otros autores y sus respectivas referencias cumplen con las pautas académicas.

Lugar y fecha:

San Miguel, 29 de noviembre de 2023

Apellidos y nombres del asesor: <u>Palomino Tofflinger, Jan Amaru</u>	
DNI: 48866095	Firma 
ORCID: 0000-0002-2076-4046	



*Este trabajo se lo dedico a mis padres y a mi hermana,
por entender que mis sueños y metas son solo míos; y a mi
abuelo David, por haber sido siempre el primero en
apoyarme en todas mis aventuras.*

AGRADECIMIENTOS

En primero lugar, quiero expresar un profundo agradecimiento a mi asesor el Dr. Amaru Palomino quien me ha guiado de inicio a fin en el desarrollo de este proyecto. Le agradezco el haber compartido toda su vasta experiencia; sus sugerencias, consejos y comentarios han contribuido inmensurablemente no solo en el desarrollo de este trabajo, sino además en mi formación, tanto personal como académica. Gracias por toda la confianza y paciencia, por esos momentos en los que resolver mis dudas promulgaba la búsqueda de aún más respuestas. Asimismo, quiero agradecer a mi co-asesor el profesor Guillermo Baldwin, por su apoyo redireccionando mis esfuerzos de investigación, por haberme acompañado durante todo el proceso compartiendo su experiencia en diseño y reflectores. Le agradezco sus preguntas, dudas y sugerencias que han aportado durante todo el desarrollo de este trabajo.

No puedo dejar de agradecer a Michael García, tanto por su apoyo en los datos suministrados para este trabajo, como por las tantas discusiones e intercambio de ideas sobre la lógica y forma detrás de la información estimada y procesada; Y a Ricardo Jiménez, por su inmenso apoyo en la adquisición de potenciales materiales reflectivos y en la implementación física y experimental de los reflectores.

Agradezco además al profesor Martin Wieser, por su apoyo en la interpretación de los datos meteorológicos, y a Álvaro Tejada y todo el Centro de Caracterización de Materiales (CAM-PUCP), por su asistencia y aporte en la medición de las características espectrofotométricas de los potenciales materiales del reflector.

Finalmente, no quiero dejar de agradecer a todos los profesores que tuve en la facultad de la escuela de Posgrado de la PUCP, gracias por la formación de calidad recibida durante estos años y por ayudarme a ver y entender cómo es que la ciencia va más allá de la teoría.

RESUMEN

En el año 2020 se produjeron un poco más de 50 mil millones de toneladas de CO₂eq a través de las diferentes industrias. 12.2 mil millones de estas fueron producto de diversos procesos de generación eléctrica. Es decir, 24.14% de las emisiones de CO₂ equivalente en el mundo son producto de la generación de la energía eléctrica. En vista de esto, uno de los avances más importantes para el control de emisiones consiste en el uso de energías renovables, siendo la energía solar unos de sus principales bastiones. En la actualidad los paneles monofaciales son los más comunes en la industria fotovoltaica. Sin embargo, según el informe de 2023 de la International Technology Roadmap for Photovoltaic (ITRPV), la participación de mercado de los Módulos Fotovoltaicos Bifaciales (BF) en 2023 es de aproximadamente el 35% y se espera que aumente a 70% para el año 2033. Además, los módulos fotovoltaicos bifaciales han abierto nuevas posibilidades para instalaciones en posiciones verticales orientadas Este-Oeste y mejorando el albedo a través de reflectores. Esta última configuración es de particular interés para el campo emergente de *agrivoltaics*. Hay poca investigación publicada sobre el rendimiento energético de módulos bifaciales en sitios de baja latitud, y todavía no se ha publicado nada para Lima, Perú. Este trabajo busca enmendar esta falta de conocimiento, buscando optimizar un arreglo BF vertical (VBF) que apunta Este-Oeste en lugar de la convención usual de módulos BF inclinados hacia el Norte en el hemisferio sur. Agregar reflectores fijos adjuntos a ambos lados del arreglo resultó en mayores irradiancias recibidas por un módulo fotovoltaico y su posterior conversión energética. Se utilizó el software de simulación óptica Tonatiuh y *bifacial_radiance* para estimar las ganancias de irradiancia a través de los reflectores para diferentes configuraciones. Luego, en el trabajo experimental subsiguiente, se utilizaron mediciones de reflectancia de diferentes materiales en un espectrofotómetro para diseñar los mejores reflectores posibles. Una vez hecho esto, se utilizó una disposición que contenía un VBF, junto con dos piranómetros adyacentes, para tomar mediciones de irradiancia recibida y energía generada a través de curvas I-V en un día de control sin reflectores. Posteriormente, se implementaron dos reflectores de aluminio a cada lado de la disposición para contrastar estas mediciones con los resultados del control. Este proceso se llevó a cabo analizando las ganancias de irradiancia y energía a través de los reflectores para días nublados y soleados típicos, con la finalidad de averiguar si había una diferencia significativa en la mejora de la producción de energía entre estos días. Los resultados indican que, después de ajustar por la variabilidad del GHI y comparado con los días de control sin los reflectores, los piranómetros instalados percibieron un promedio de 59% más irradiancia en días soleados y 32% más en días nublados. Asimismo, utilizando las Curvas I-V del módulo, se pudo observar una mejora considerable de un promedio de 39% mayor entrega de máxima potencia para días soleados y 21% en días nublados.

Enhancing the energy yield of a vertical bifacial photovoltaic module through the implementation of fixed aluminum reflectors

David Elias Nuñez Rishmawi

Abstract—

In the year 2020, just over 50 billion tons of CO₂eq were produced across various industries. 12.2 billion of these were the result of various electrical generation processes. This means that 24.14% of the world's equivalent CO₂ emissions are the result of the generation of electrical energy. In light of this, one of the most important advances for emission control is the use of renewable energies, with solar energy being one of its main strongholds. Currently, monofacial panels are the most common in the photovoltaic industry. However, according to the 2023 report by the International Technology Roadmap for Photovoltaic (ITRPV), the market share of Bifacial (BF) PV Modules in 2023 is about 35% and is expected to increase to 70% by 2033. Additionally, bifacial PV modules have opened new possibilities for installations in vertical positions facing East-West and enhancing the albedo through reflectors. This latter configuration is of particular interest to the emerging field of agrivoltaics. There is little published research on the energy yield of bifacial modules at low-latitude sites, and nothing has been published yet for Lima, Peru. This work contributes to amending this lack of knowledge, seeking to optimize a vertically installed BF (VBF) arrangement that points East-West instead of the usual convention of inclined BF modules facing North in the southern hemisphere. Adding fixed reflectors attached to both sides of the arrangement yielded higher irradiances received by a photovoltaic module and its subsequent power conversion. Optical simulation software Tonatiuh and bifacial_radiance were used to estimate the irradiance gains through the reflectors for different configurations. In the subsequent experimental work, reflectance measurements of different materials in a spectrophotometer were used to design the best possible reflectors. Once this was done, an arrangement containing a VBF was used, along with two adjacent pyranometers, to take measurements of received irradiance and generated power through I-V curves on a control day without reflectors. Subsequently, two aluminum reflectors were implemented on each side of the arrangement to contrast these measurements with the control results. This process was carried out by analyzing the irradiance and power gains through the reflectors for typical cloudy and sunny days to find out if there was a significant difference in the improvement of energy production between these days. The results indicate that, after adjusting for GHI variability and compared to the control days without the reflectors, the installed pyranometers perceived an average of 59% more irradiance on sunny days and 32% more on cloudy days. Likewise, using the I-V Curves of the module, a considerable improvement of an average of 39% greater maximum power delivery for sunny days and 21% on cloudy days could be observed.

INDEX

Abstract.....	5
I. INTRODUCTION.....	7
II. MATERIALS & SOFTWARE	10
III. METHODS & DESIGN	12
IV. RESULTS	22
VII. CONCLUSIONS.....	39
REFERENCES.....	41



I. INTRODUCTION

Bifacial PV (BF) modules were first commercially manufactured in 1983, but their share in the common PV market wouldn't go up until recent years [1]. Currently and according to the International Technology Roadmap for Photovoltaic (ITRPV) the market share for BF modules is about 35% for the year 2023, and it is expected to grow to 70% by the year 2033 [2]. This means that improving the energy yield and conversion of BF arrays will increase in impact as the decade progresses.

One type of novel configuration for solar modules in the current literature is the Vertically Mounted Bifacial (VBF) PV modules, which as the name implies, are installed perpendicular to the ground plane. This differs from conventional BF and MF installations, which in Peru are usually tilted 15 degrees, facing North. Both Configurations can be seen in Fig. 1.

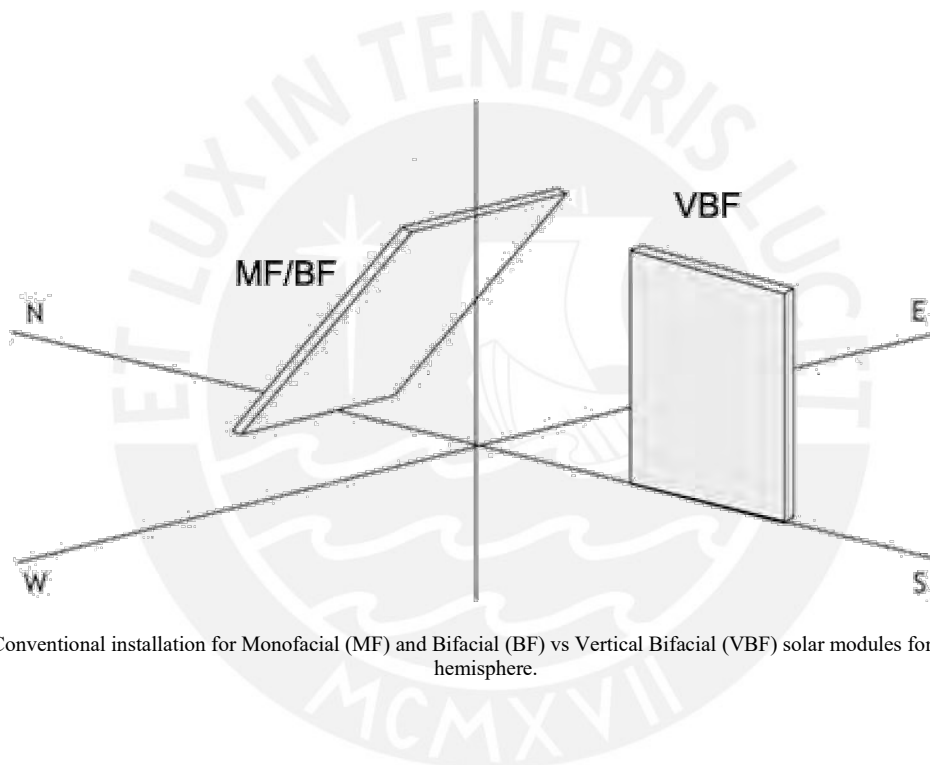


Fig. 1. Conventional installation for Monofacial (MF) and Bifacial (BF) vs Vertical Bifacial (VBF) solar modules for the southern hemisphere.

VBF main advantages come from reducing the effect of soiling loss of the modules [3], [4], [5] and improving the energy conversion at the beginning and the end of the sun hours. Applications for this type of system has been vastly explored in *agrivoltaics* [6], [7], [8], where both solar modules and agriculture activities use the same area of land simultaneously. An illustrative figure of this last effect is presented in Fig. 2.

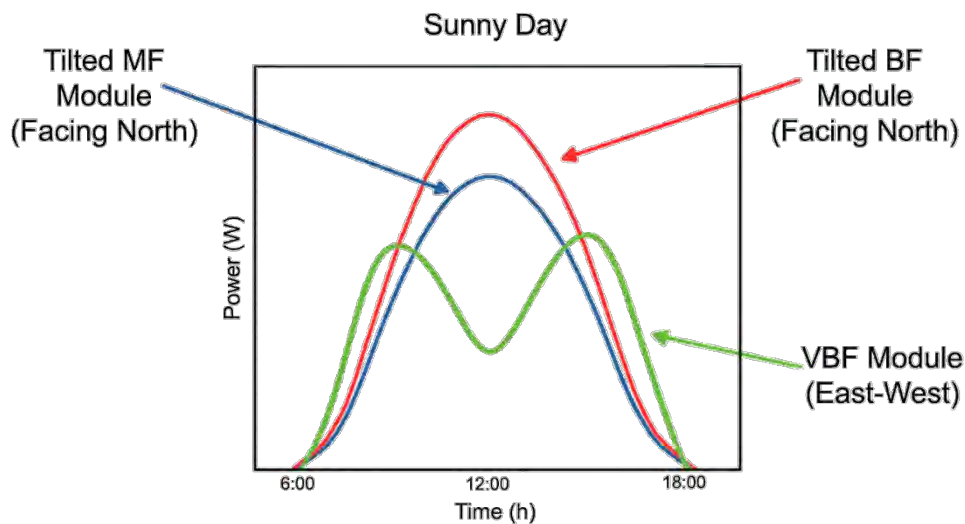


Fig. 2. Theoretical Power over time for different types of PV modules. In blue a conventional tilted Monofacial (MF), in red a tilted BF and in green a E-W VBF.

However, as described in [9] the increment in yield of VBF compared to BF or even Monofacial Solar Modules (MF) varies greatly depending on the latitude of the location, as well as the albedo and the sky conditions. Based on their simulations, it is theorized that a VBF installation in low latitudes, such as in Lima, Peru, may not be the optimum array configuration to install. The present research was put in motion to verify this hypothesis experimentally.

One of the main advantages of BF, in general, is that they are able to receive solar energy reflected by the ground [10] [11]. This opens two controllable variables on which the energy yield depends: the ground's material (and hence its reflectivity) and its geometry or orientation.

For instance, in [12] a mathematical model was designed to estimate the increase in yield of a BF taking into consideration the ground reflectivity, among others and it was deemed as an input imperative to appropriately calculate the energy generation of BF modules.

Johnson & Manikandan [13] simulated energy production of different BF arrays using PVsyst, a well-known PV software used for simulations. They used Kattankulathur, India as the location, which is about 13° North in latitude, just 1° shy of the inversely located Lima, which is 12° South in latitude. Interestingly, their results indicate that between all the tested configurations, a South Facing module tilted 13° yielded the best results in Total Power produced within a simulated year.

These results are cohesive with the experimental results of the work made by Muthu & Ramadas [14] whose results indicate that a South facing VBF is optimal for the winter months in Minjur, Tamil Nadu, India, while an East facing VBF yielded the best results in the summer months. Minjur is located at a latitude of 13.27° north, very close to Kattankulathur (Approximately 56 km to North).

The aforementioned configuration, however, differs from the arrangement of the modules installed at the university roof where the study is being conducted, which has their modules vertically installed and facing west.

In [15] another simulated energy production was explored using PVsyst, but only for two BF configurations: Tilted facing south and VBF facing east with the latter granting better results.

On the other hand, [16] explored the albedo as a major component of the energy output of bifacial modules. It was done by designing an In-House Ray Tracing Software to evaluate albedo and as a result, potential reflector materials. They compared perfect Specular Reflectors against perfect Diffuse Reflectors, concluding that Diffuse Reflectors yielded the best results. However, this was only tested for beams of light with an angle of incidence of 85° so the conclusion is very limited.

In relation to this, [17] and [18] analyzed the effect of albedo more in-depth, concluding that the spectral albedo of the materials is more relevant than the effective albedo when predicting energy output. While they mostly examined conventional materials found in PV installations, their methodology influenced the material selection process present in Chapter III of this research.

However, there is not much literature exploring the influence that ground geometry has on the energy yield of BFs. The most significant being [19], an article presenting the viability of ground sculpting. They explored the possibility of angling the ground around a VBF multi-array system in different ways to improve its yield. Their model suggest that Ground sculpted VBF work best for higher latitudes, even showing that below 20° of latitude a conventional MF array tends to yield better than VBF configurations.

More recently, [20] used two typical mirrors to enhance the yield of one single VBF, by manually tilting the mirrors in hourly at a latitude of 37° North (South Korea). Their results turned out to be promising, enhancing the peak power generation of the array by up to 51% for the entire year as compared to the same system without the mirrors.

With the above-mentioned literature in consideration, the main effort of the present research is to improve both of the previously described variables. Designing and implementing specialized reflectors and mounting them in a configuration of VBF. This proposed array will have the nomenclature of Vertically Mounted Bifacial Solar Modules with Specialized Reflectors, or rVBF for short. Considering the previous studies, this system should have a significant increment in yield compared to more conventional MF or even BF installations.

II. MATERIALS & SOFTWARE

A. System and materials

One commercial BF module was installed vertically facing west. Additionally, two pyranometers were installed vertically and adjacent to the modules, one facing east and the other facing west.

The Solar module has a height and width of 1.696m and 0.992m respectively. This module is a monocrystalline bifacial Passivated Emitter Rear Cell (PERC). with half-cut cells, a maximum power of 320 W at standard test conditions (STC), and a power bifaciality of $(73\pm 5)\%$, according to the manufacturer's data sheet. The VBF was connected to the lab's capacitive load-based I-V curve tracer. The current and voltage were measured with two Keysight 34465A multimeters, and the subsequent I-V curve was measured at five-minute intervals between each measurement. From this I-V curve, the maximum power was extracted for the calculations in Chapter IV.

Adjacent to the module and facing the same orientation, two EKO MS-80M pyranometers were located in order to measure the incident irradiance on the west-oriented front and the east-oriented back side. Additionally, an extra pyranometer was installed facing up (towards the zenith angle) to measure the GHI of all measured days and select the ones that mostly resemble ideal sunny or cloudy conditions. The irradiance perceived by either of the pyranometers was measured at the beginning and end of the module's I-V curve tracing.

A picture of the system, before the reflectors were installed, is shown in Fig. 3. Highlighted in red are the module and pyranometers (one on either side) that would be used in the study.

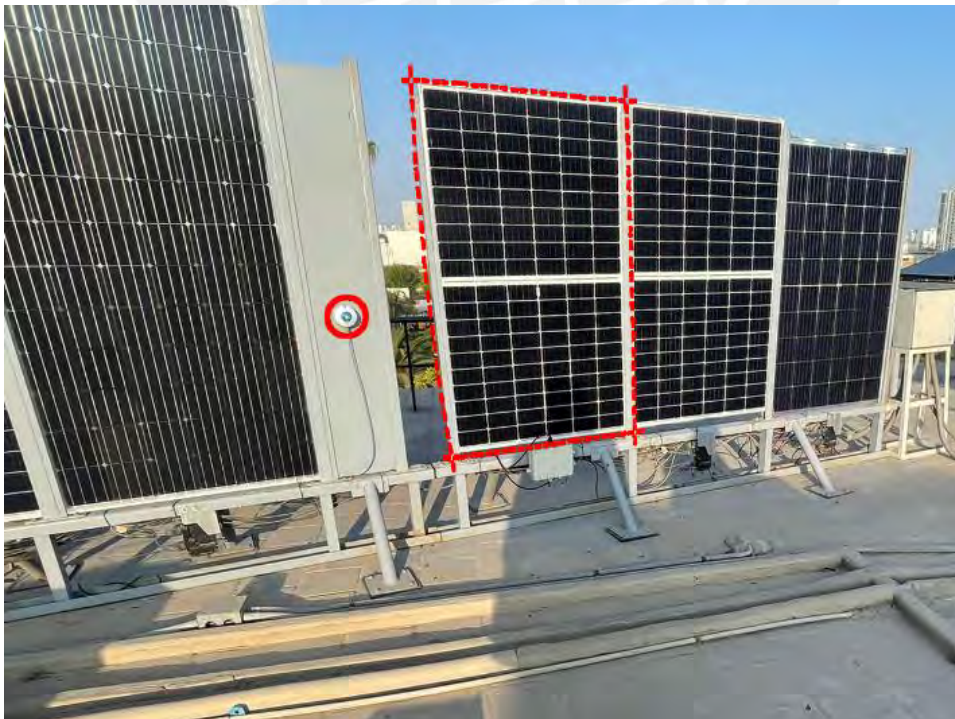


Fig. 3. Picture of the west-facing side of the module and its corresponding pyranometer

The reflector material, design, and optical characteristics are further explored in Chapter III. Both the modules and pyranometers have been collecting power and irradiance data since early 2022.

B. Software

Two key software were also utilized for the design of the reflectors: Tonatiuh (solar concentrator and ray tracing software) [21] and bifacial_radiance (a NREL tool that aids in the simulation of bifacial systems) [22].

Tonatiuh was useful in determining the geometrical dimensions of the reflectors (seen in Chapter III), while bifacial_radiance would prove beneficial for determining the optimum tilt of the reflectors for maximum yield (Chapter IV).



III. METHODS & DESIGN

A. Irradiance Calculation

A plethora of different models to determine the total irradiance on a surface have been developed over the years [23], [24]. However, most of them utilize three main variables that equate to the total irradiance received by a surface (G_t), them being the direct irradiance coming from the sun (G_d), the irradiance that was ground reflected (G_r) and irradiance product of the scattering of sunlight in the sky (G_s). An image of this concept is presented as Fig. 4.

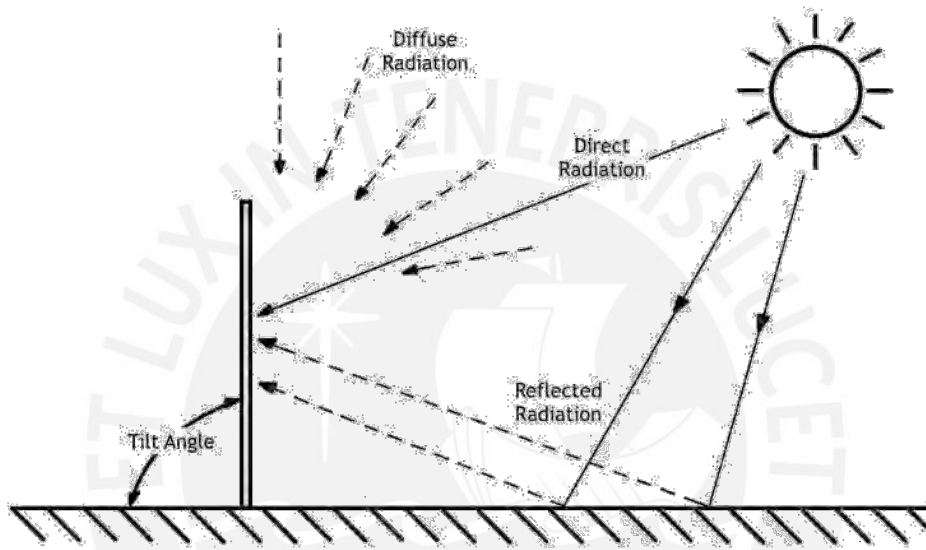


Fig. 4. Visual representation of the three main components that add to the Total Irradiance in a surface (G_t): Diffuse Irradiance (G_s), Direct Irradiance (G_d) and Reflected Irradiance (G_r)

Each of these Irradiance measurements are generally a factor of common irradiance measurements. Global Horizontal Irradiance (GHI) and Albedo factor are used to calculate G_r ; Direct Normal Irradiance (DNI) for G_d and Diffuse Horizontal Irradiance (DHI) for G_s , with each of factors account for G_t vary according to the depth of research and technology available [23]. More broadly, Eq. (1) is presented as a simplified relation between these concepts:

$$G_t = G_d + G_r + G_s$$

With this, we understand that to optimize the reflector configuration properly, we must consider all three types of irradiances when possible.

B. Reflector Geometry

Three primary geometries were initially contemplated for the solar reflectors: flat, parabolic, or perhaps hyperbolic. While freeform reflectors have been utilized in PV designs before, especially in high-

concentration photovoltaics [25], these are usually applied to small solar cells, not whole modules, and come with complexities not worth further exploring for the prototype of the present experiment.

On the other hand, reflectors with parabolic (or even hyperbolic) surfaces are common applications for solar concentrator or concentrator photovoltaics [26], [27], [28], [29], as they take the incident solar rays and redirects them on a small linear or circular surface. However, while this should be feasible for a large-scale implementation (such as on an entire solar module), the dimensions of the reflectors would prove unpractical for that level of concentration.

Furthermore, for a solar module to optimally convert light into power, all solar cells must be illuminated as evenly as possible to not form unnecessary resistances within its own circuit [30]. The most practical method to do this is by using flat reflectors. This means the incident rays keep their plane wavefronts as they are being redirected to illuminate the module as evenly as possible, although with some parasitic reflection present [31].

While curved reflectors have been implemented before [32] this was only done for tilted MF arrays facing south, where the sun path makes the angle of the incident rays not vary as much while also taking advantage of the spacing between modules of the MF system, where the backside presents no issue by being covered. This is not the case for the present study, as it involves a different configuration and goal.

Taking this into consideration and examining the simplicity of the ideal implementation, as well as previous successes by similar studies like [20] and [33], flat reflectors are preferred, and this was the starting point for the rest of its characteristics.

C. Reflector Dimensions

The reflector dimensions are mainly a product of the sun's path, which is never perfectly aligned from east to west and predominately exhibits a zenith angle different from 0. This angle varies depending on the location's latitude and date of the year, but always maximizes in both the winter and summer solstices. For the lab coordinates in Lima, the sun has a minimum zenith angle of around 35° (to the North) in the winter solstice and 12° (to the south) in the summer solstice at 12:15 p.m. A diagram of a sun position is presented as Fig. 5.

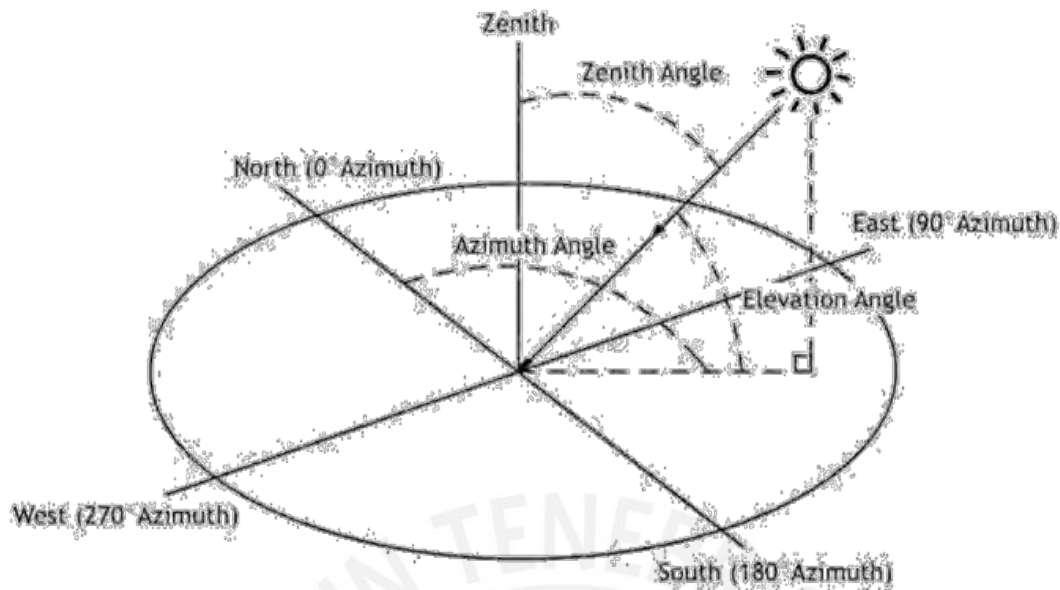


Fig. 5. A visual representation of the sun position, which can be described by the Zenith, Azimuth and Elevation Angles.

For the experiment's location, the sun, at its highest elevation will always be tilted towards North from February 18th to October 25th and to the south from October 26th to February 17th.

This means that to effectively distribute Direct Normal Irradiance the reflectors cannot have the same width as the VBF, as this would mean a non-homogenous lightning of the module. To illustrate this a simulation has been run in the software Tonatiuh, where a system of a VBF facing west and a single planar reflector with a 25° inclination has been build, seen as Fig. 6.

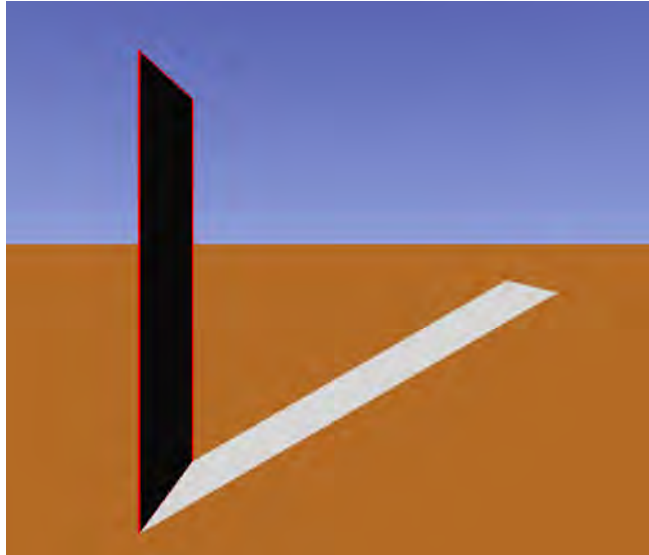


Fig. 6 Tonatiuh model of a VBF facing west and a single planar reflector with a 25° inclination.

With this system, a ray tracing simulation was executed, and the corresponding incident flux distribution is shown Fig. 7. Fig 7(b) shows the flux distribution of a perfect sun path from east to west with 0° of Zenith angle and Fig 7(a) demonstrates a more real occurrence, where the sun is at its highest elevation in the winter solstice. Both figures denote graphically which segments the solar panel get illuminated because of the reflection. For instance, Fig 7(a) shows an ununiform illumination pattern due to the Sun's Zenith angle.

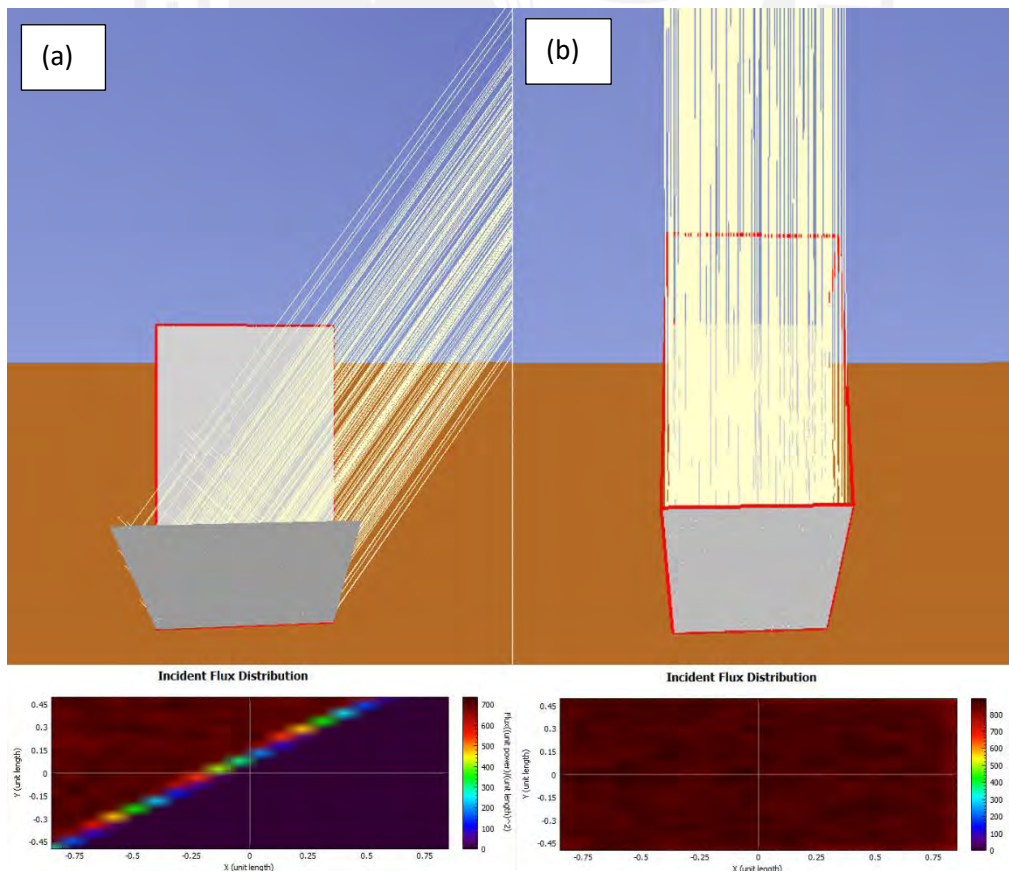


Fig. 7 Incident flux distribution for a reflector of the same width as the VBF. (a) Sun at its highest elevation in Lima, Peru during winter solstice. (b) Theoretical sun position that assumes 0° Zenith and 90° Elevation.

As seen in the figure above, the elevation angles have a more than sizable impact the reflectors' efficiency, and this effect maximizes the farther it is from the equator. To account for this notion, the reflector should be wider than the module, to illuminate the whole VBF uniformly. Since this angle is maximized for North and South in the winter and summer solstices, respectively, those dates were considered when designing the dimensions of the module. Fig 8. shows the result of the reflector taking this concept into account, presenting the reflections for the summer (Fig 8(a)) and winter (Fig 8(b)) solstices.

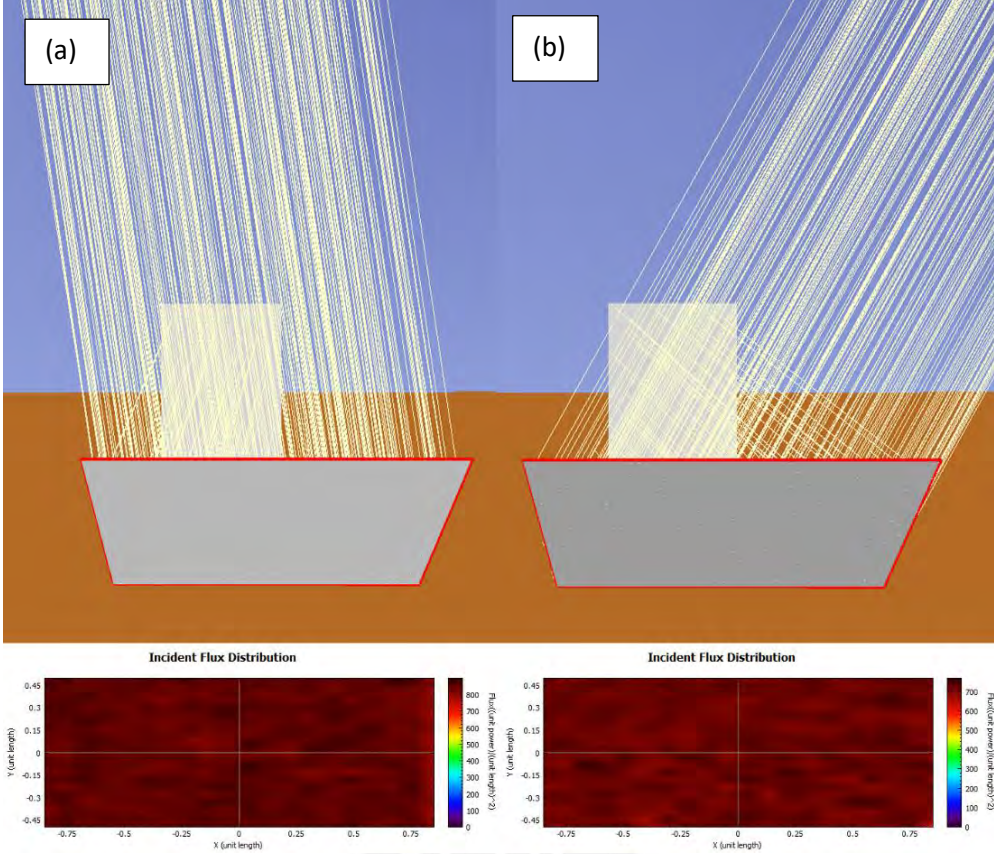


Fig. 8 Incident flux distribution for a reflector of the optimal width. (a) Sun at its highest elevation in Lima, Peru during summer solstice. (b) Sun at its highest elevation in Lima, Peru during winter solstice.

This concludes that, for the reflectors to be fully effective all year round, they should extend at least 1.16m to the north and 0.36m to the south of the edges of the target VBF for the experiment's location. This means that for a module of 0.996m in width, the reflectors ought to be 2.516m wide.

However, for practicality, and since the present experiment would not be carried out all year round, the reflectors would be designed to be movable, and their length would be decided according to the availability of commercial materials.

D. Reflector Materials

Different commercial materials were readily available for implementation. A sample of each of them was cut out in order to test them in a spectrophotometer. The sample materials can be seen in Fig. 9(a) with a picture of the measuring device in Fig. 9(b)

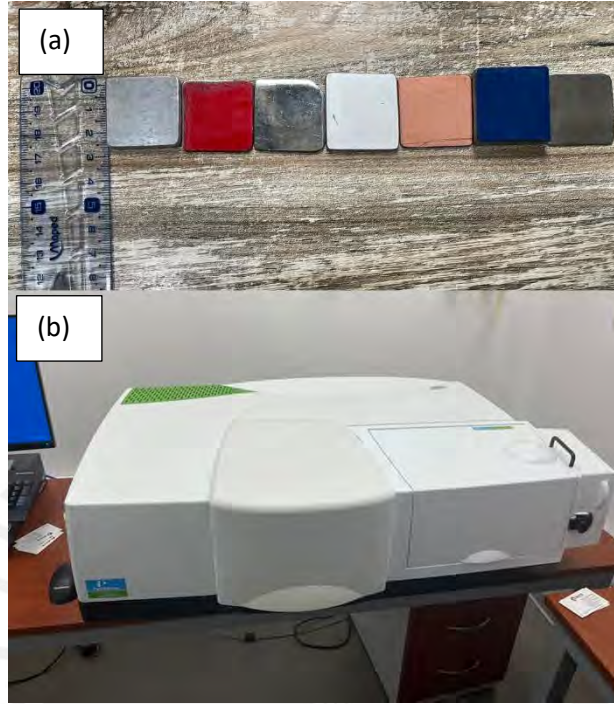


Fig. 9 (a) Materials tested from left to right: Aluminum I, Epoxy Red, Chrome Steel, Aluminum II, Copper, Epoxy Blue, Stainless Steel. (b) Spectrophotometer used for the experiment.

Two aluminum samples were chosen. Aluminum I had more direct reflectance while Aluminum II was more diffused. Both Epoxy Red and Epoxy blue are also Aluminum sheets but covered with epoxy resin of red and blue tones respectively. On the other hand, 2 Steel samples were chosen, Chrome Steel having more direct reflection over the Stainless Steel. The final sample was a readily available Copper sheet.

The measurement device was a UV/VIS/NIR spectrophotometer from Perkin Elmer, model Lambda 950. It uses an integrating sphere made from Spectralon, with a diameter of 150 mm, with two detectors: A photomultiplier tube (PMT) for the UV and visible range and a photodiode of InGaAs for the infrared range. With this configuration, the device measures a spectral range from 200 nm to 2500 nm with intervals of 5 nm to estimate the sample material's spectral reflectivity (R). Fig. 10 shows the different R curves for each sample material at different wavelengths, and Table I shows the average reflectance for the whole spectra (overall reflectance) as well as the average reflectance of the usable PV range (200nm - 1200nm).

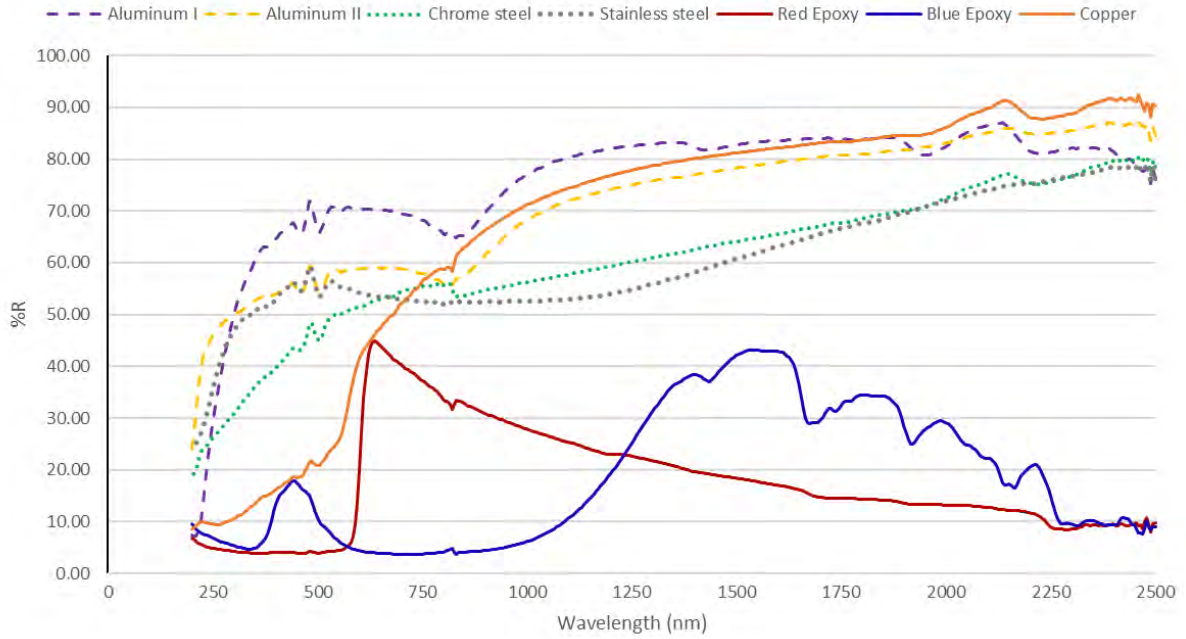


Fig. 10 Spectral reflectivity for each material. Read as how much of a percentage of the incident ray of light was reflected in total (both directly and diffusely) for each unit of wavelength, measured each 5 nm.

TABLE I
Average Overall Reflectance and Usable Reflectance for Each Material

<i>Material</i>	<i>Overall Reflectance(%)</i>	<i>Usable Reflectance(%)</i>
Aluminum I	75.59	66.22
Aluminum II	71.82	59.22
Chrome Steel	60.74	51.33
Copper	67.64	48.82
Epox Red	17.39	45.36
Stainless Steel	60.72	20.90
Epox Blue	18.48	7.57

However, since the focus is on the spectra that the solar module can convert into energy, it is important to take into consideration the spectral density of the irradiance on Earth's surface instead of just maximizing for total reflectance. That is, consider the density of available photons Fig. 11 represents such spectra.

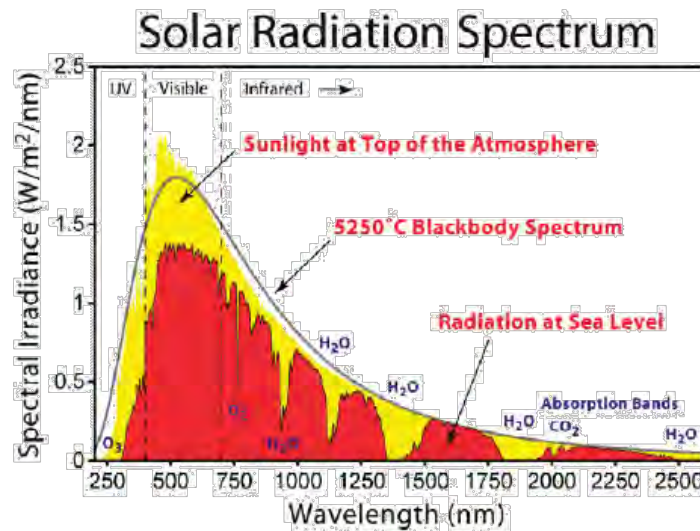


Fig. 11 Spectral Solar Irradiance at atmosphere and sea level for an Air Mass of 1.5. Source [34]

Here, it is evidenced that of the whole solar spectrum that reaches the earth's surface, each wavelength carries different amounts of Irradiance with high degrees of variability. So, to more accurately select a reflector material, the spectral reflection should be taken into consideration since it is more important relevant than the overall effective reflection [17], [18]. To do this, Fig. 12 was constructed by multiplying the spectral density of sea level radiation available from the database of the National Renewable Energy Laboratory (NREL) [35], with the %R (Reflectance) component (Fig. 12) for each nanometer measurement available (every 5 nm). Table II represents the integrated amount of reflected irradiance for both the overall (200nm - 2500nm) and usable ranges (200nm – 1200nm).

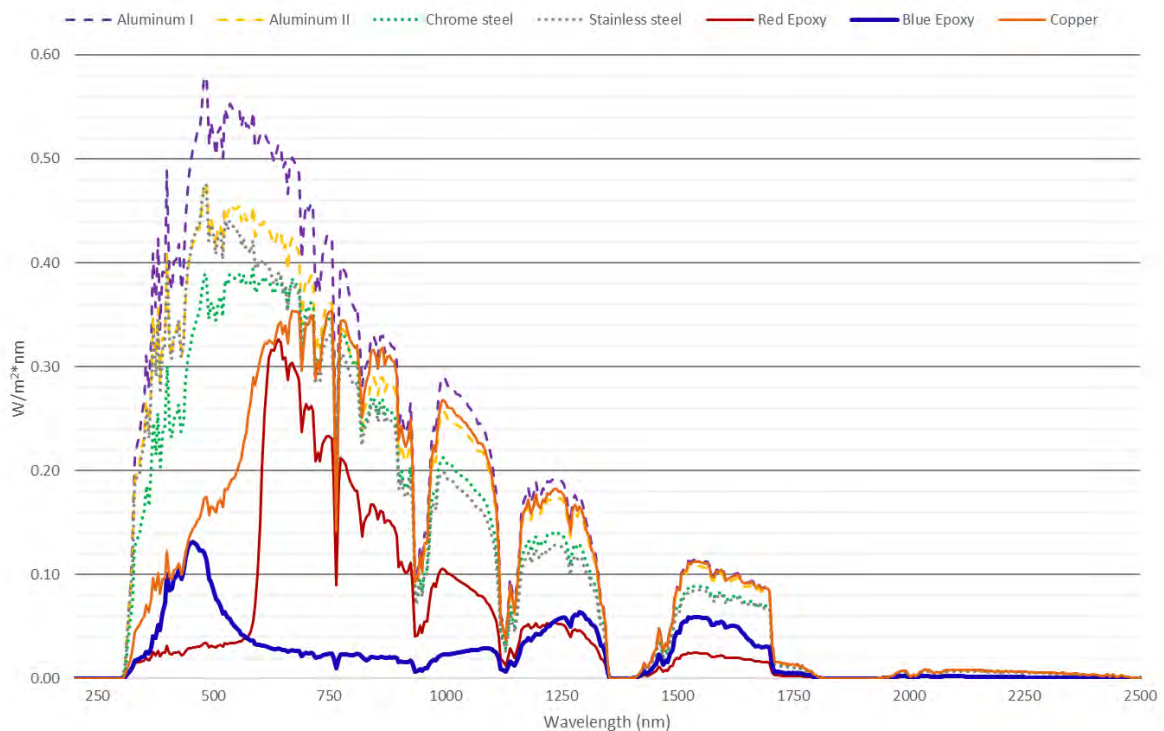


Fig. 12 Weighted spectral reflectivity for each material.

TABLE II
Average Overall Reflected Irradiance and Usable Reflected Irradiance for Each Material

<i>Material</i>	<i>Overall Reflected Irradiance (W/m²)</i>	<i>Overall Usable Irradiance (W/m²)</i>
Aluminum I	355.61	305.82
Aluminum II	307.17	260.56
Chrome Steel	271.75	235.77
Stainless Steel	260.89	222.69
Epoxy Blue	240.19	191.85
Copper	106.89	95.44
Epoxy Red	51.90	32.40

While the data was constructed using the radiation for an Air Mass of 1.5, which varies with sun elevation as well as with latitude and longitude of each location, it is a fair approximation for the goal of selecting the best material for implementation.

With the previous results and prioritizing maximum usable reflectivity, the material from the sample in Aluminum I plate was chosen for the experimental implementation for the reflector.

E. Final Design

All the previous points were taken as a baseline for the final design. However, for material availability and cost reasons, the reflectors' dimensions will not be equal to those calculated previously. The largest commercially available plates from the selected material have a height and width of 1.2m and 2.4m, respectively. In order to properly construct two reflectors, one for each side, three of these plates were acquired. One of the plates was carefully divided in half to add up to two plates of 1.8m in height and 2.4m in width.

These aluminum plates were then mounted on a support structure and affixed to the existing VBFs structure. Since the tests were to be performed between the months of April and June, and according to the simulation in Chapter III. Extra width towards the North of the module was needed.

The final design was then constructed in Solidworks, and is presented in Fig. 13 and Fig. 14



Fig. 13 East (Lateral) view of the VBF, reflectors and pyranometers.



Fig. 14 South (Frontal) view of the VBF, reflectors and pyranometers.

IV. RESULTS

To discuss both simulated and experimental results, Table III is presented as a summary of the various parameters that would be used to assess the performance of the system with and without the reflectors.

TABLE III
Parameters for Performance Analysis

<i>Parameter</i>	<i>Symbol</i>	<i>Note</i>	<i>Formulae</i>	<i>Units</i>
GHI Reference Yield	Y_r^{GHI}	It is the number of hours at the reference irradiance as read by a zenith facing pyranometer, because of this, it remains unaffected by the installed reflectors.	$Y_r^{GHI} = \frac{H^{GHI}}{1000W/m^2}$	kWh/kW/day
East Reference Yield	Y_E	It is the number of hours at the reference irradiance as read by the east facing pyranometer next to the module.	$Y_E = \frac{H^E}{1000W/m^2}$	kWh/kW/day
West Reference Yield	Y_W	It is the number of hours at the reference irradiance as read by the west facing pyranometer next to the module.	$Y_W = \frac{H^W}{1000W/m^2}$	kWh/kW/day
Module Reference Yield	Y_r^{E+W}	It is the number of hours at the reference irradiance as read by the sum of the east and west facing pyranometers next to the module.	$Y_r^{E+W} = \frac{H^\perp}{1000W/m^2}$	kWh/kW/day
Array Yield	Y_P	It is the time (in hours) taken by the PV module to generate energy at its nominal power. Formulated by Dividing the energy output over the module's nominal power at STC.	$Y_P = \frac{E^\perp}{320W}$	kWh/kW/day
GHI Performance Ratio	PR^{GHI}	It is the performance of the solar module. Formulated as the ratio of the Array Yield over the GHI Reference Yield.	$PR^{GHI} = \frac{Y_P}{Y_r^{GHI}}$	%
Module Performance Ratio	PR^{E+W}	It is the performance of the solar module. Formulated as the ratio of the Array Yield over the Module Reference Yield.	$PR^{E+W} = \frac{Y_P}{Y_r^\perp}$	%

A. Simulated results

To calculate the irradiance experienced by the experimental system, the ideal inclination of the reflectors described in Chapter III is needed. For this purpose, simulations within the software `bifacial_radiance` were designed.

With this software, a set of two reflectors was constructed approximating the characteristics of the final design calculated in Chapter III. The objective was to simulate the total irradiance received over time by one VBF module, and then compare the same arrangement with reflectors on both sides (rVBF). The module was simulated with its physical dimensions of 1.696m tall and 0.992m wide. On the other hand, the reflectors were simulated using the plate's dimensions of 1.8m tall and 2.52m wide to appropriately reflect the sun during its yearly path, as simulated in Chapter III.

The reflection coefficient of the reflectors was set to 0.75 to simulate the aluminum's reflectance integrated across available sunlight wavelengths (200nm - 2500nm), derived beforehand in the material section of Chapter III. When the reflectors are not considered, the ground was simulated with an albedo

of 0.23. To obtain this albedo, a prior test was conducted on the surface of the roof where the solar modules are installed.

During the month of May two pyranometers were installed: One facing upwards (towards the Zenith) and the other downwards (towards the ground), to appropriately measure the effect of the reflection of the ground and as such, calculate the albedo per time of the day. This effective albedo was calculated as division between the of the irradiation received by the pyranometer facing towards the Zenith (P_z) and the irradiation perceived by the pyranometer facing the ground (P_g) per unit of time (measured every 30s) With this, Fig. 15 depicts the albedo using a sample sunny day (7th of May of 2023) from the batch of data.

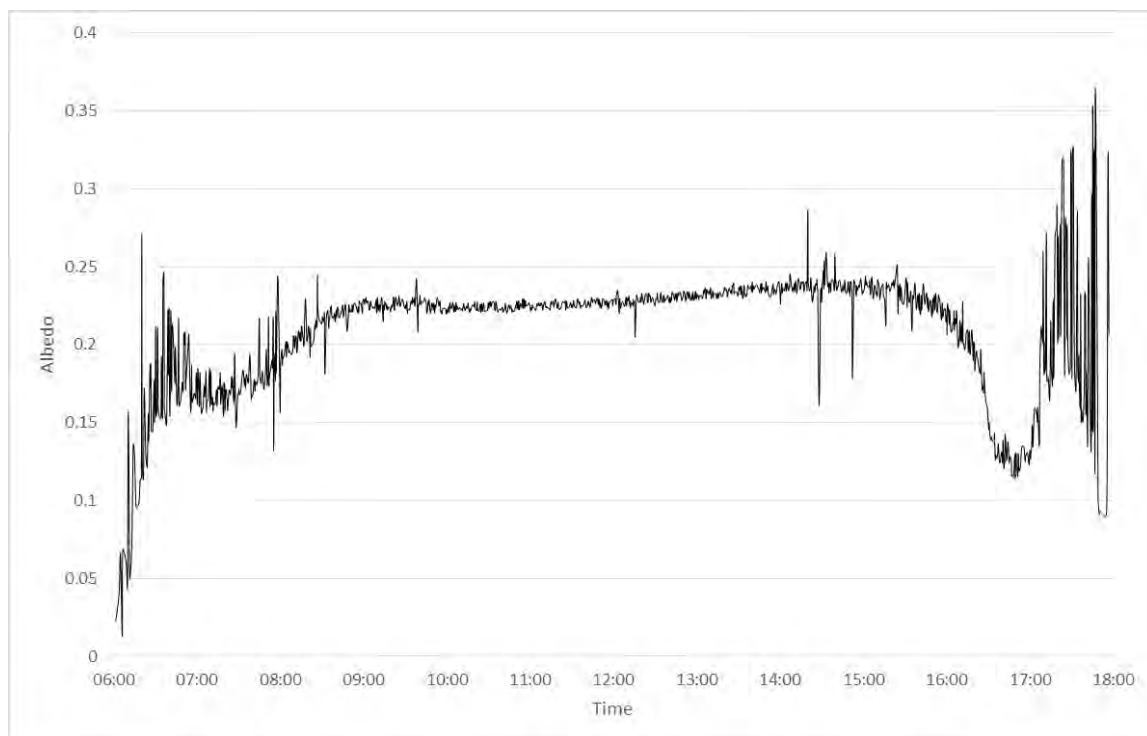


Fig. 15 Ground albedo as a function of time

From here, it is evidenced that the early morning and late afternoon give noisier readings. This is likely due to the low irradiances at shallow sun elevation at sunrise and sunset and the optical impact of other objects on the rooftop. Because of this, only the measurements at higher elevations within the time between 8:30 in the morning and 16:00 in the afternoon were used. This way, an average albedo of 0.2285 was found (rounded up to 0.23 per simulation purposes).

To find the ideal inclination of the reflectors, the simulation was run first with three different possible inclinations: 20, 25 and 30 degrees.

The results were finally simulated with the following parameters: The simulation was run first with the reflectors and then without them. Both systems were simulated using the hourly irradiance of two different days of a typical meteorological year in Lima, Peru obtained from [36], the 19th of January (for a typical sunny day) and the 21st of June (for a typical cloudy day). The solar module 1.696m tall

and 0.992m wide in the middle, with 75% overall reflectance mirrors adjacent to it at various tilting degrees. The ground was set to have an albedo of 0.23.

Visual representations of the simulated arrangement using `bifacial_radiance` are presented in Fig. 16 and Fig. 17.

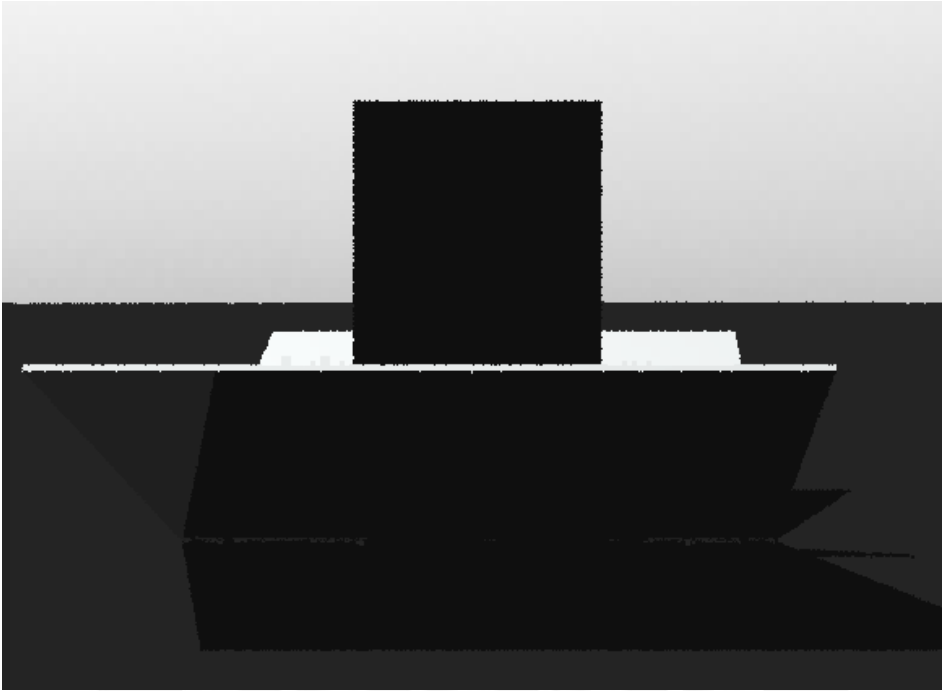


Fig. 16 East (Lateral) view of the simulated VBF and reflectors.

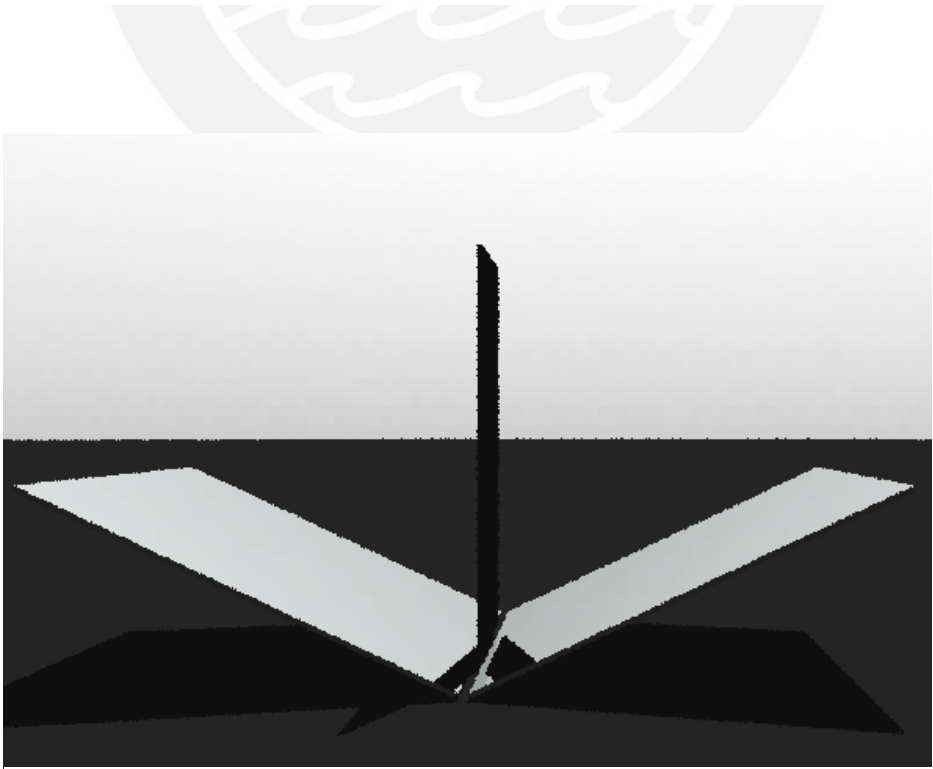


Fig. 17 South (Frontal) view of the simulated VBF and reflectors.

The experiment was run three times per day, changing the tilt angle of each reflector. Using these simulations, Table IV was constructed:

TABLE IV
Simulated Module Reference Yield for Different Reflector Tilt at Cloudy and Sunny Days.

System	Cloudy Day		Sunny Day	
	Y_r^\perp	Increment(%)	Y_r^\perp	Increment(%)
Without reflectors	2.21	0%	7.07	0%
Reflectors 20°	2.72	23.15%	8.06	13.98%
Reflectors 25°	2.75	24.34%	8.26	16.87%
Reflectors 30°	2.73	23.21%	7.37	4.27%

From this table it is deduced that the optimal angle for installation would be 25°, with an increased percentage of 24.34% and 16.87% in total received irradiance for the cloudy and sunny day respectively.

With this information, an hour-to-hour irradiance was calculated through additional simulations for both sides of the module and are presented as Fig. 18 for the sunny day and Fig. 19 for the cloudy day.

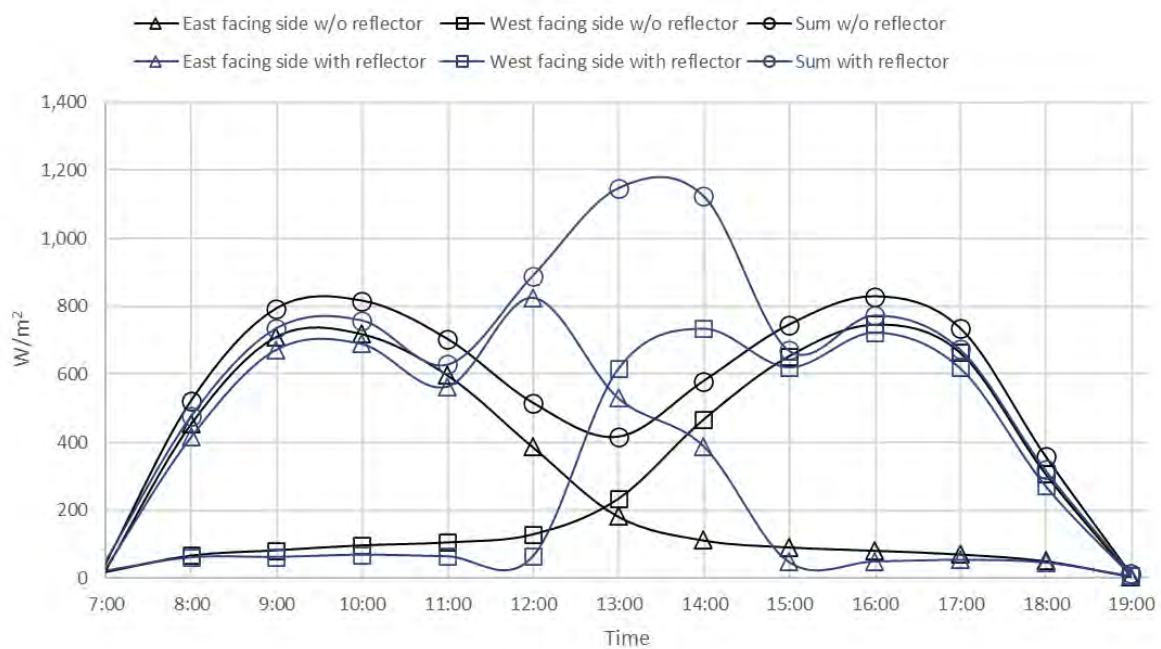


Fig. 18 Simulated hourly irradiance received by the VBF with and without reflectors on a sunny day.

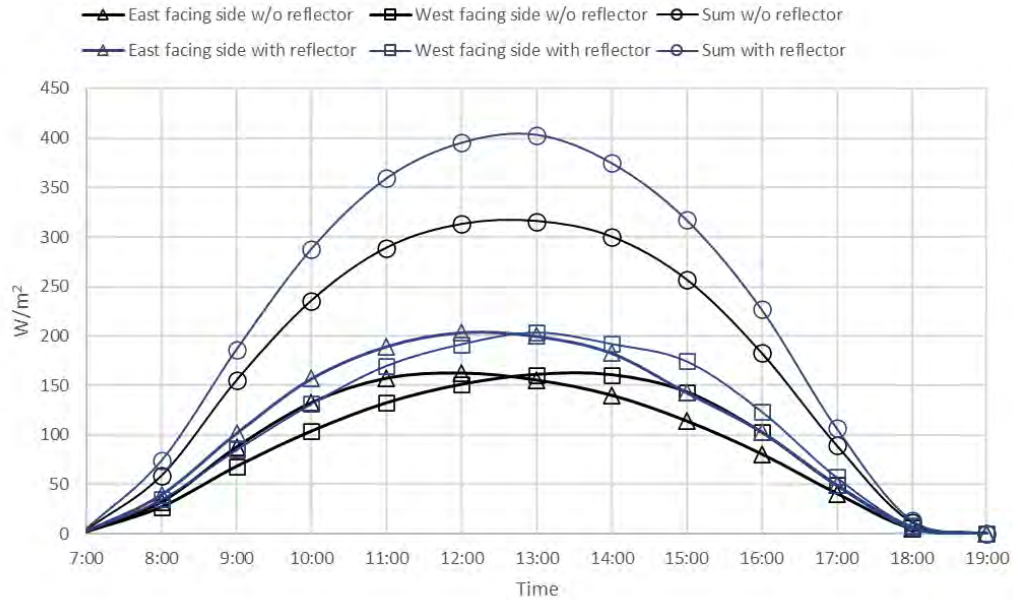


Fig. 19 Simulated hourly irradiance received by the VBF with and without reflectors on a cloudy day.

With these results, the simulation was run to add up for a whole year, altering the height (H) of the array and the reflectivity (R) of the reflectors. The Module Reference Yield of the different configurations is presented in Fig. 20.

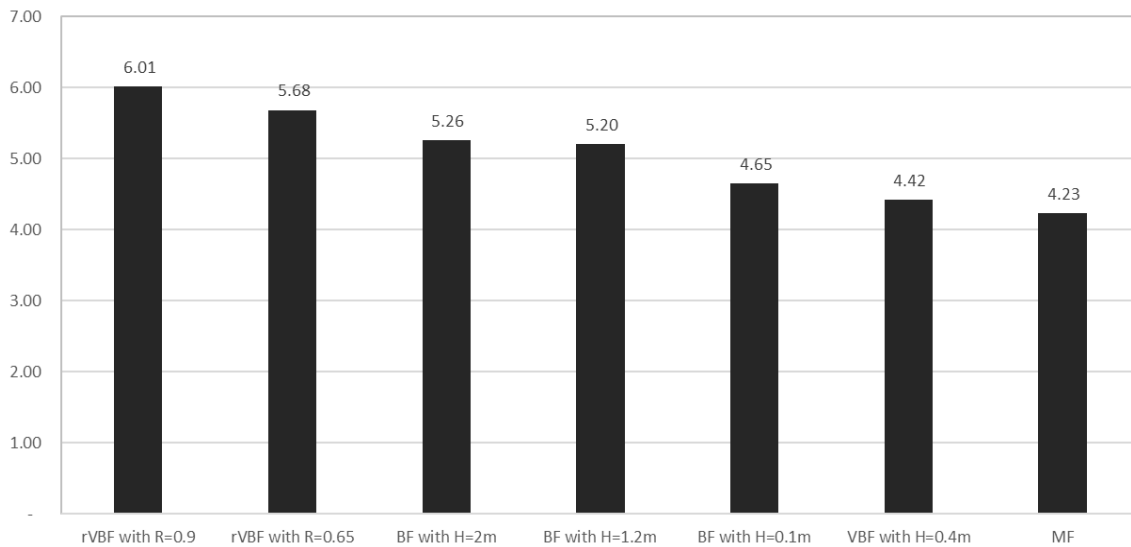


Fig. 20 Yearly averaged Module Reference Yield for each configuration. R denotes the overall reflectance of the reflectors and H the height (distance from the ground) of the lowest part of the module.

In Fig. 20, rVBFs with reflective coefficients of 0.65 and 0.9 are simulated. Additionally, conventional BF (tilted 15° facing North) were simulated at an elevation of 0.1m, 1.2m and 2m from the ground. The first elevation imitates conventional installations at roof level, the second elevation

simulates a module already installed at the roof of the university’s physic department, which is also where the experiment was conducted. The final elevation of 2m was used because little to no gain is obtained from elevating the module farther than this point per the simulations.

The simple VBF without any reflectors was simulated with an elevation of 0.4m, also to replicate the array that is currently installed at the roof. Finally, a conventional MF (tilted 15° facing north with 0 elevation) was simulated to have a baseline.

All these configurations exhibit a positive yield compared to the conventional MF array and these results are presented on Fig. 21.

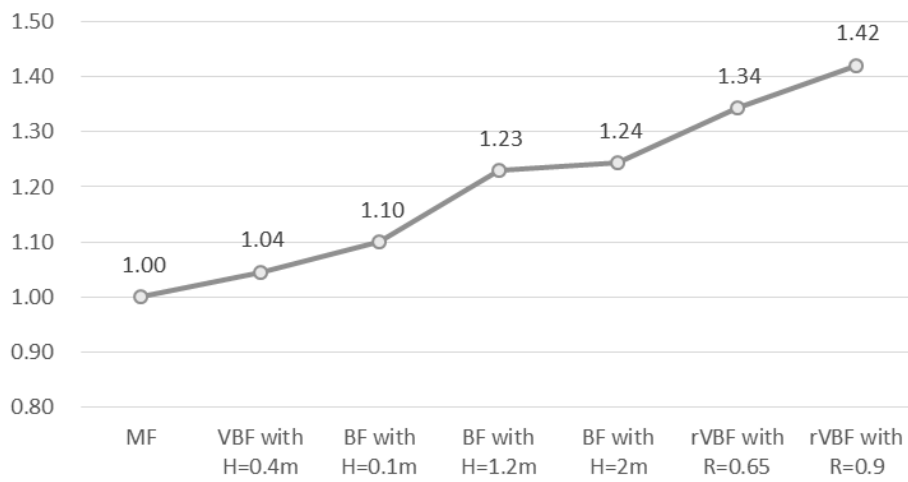


Fig. 21 Simulated reference yield increment among different configurations.

As displayed, irradiance perceived by the VBF module is up by 4% with respect to the MF baseline, but way below the 10% yield of the conventional BF for our location in Lima. However, according to these results, a Yield increment 34% is expected of an rVBF with reflectors with an average of 0.65 reflectivity with respect of the MF; Significantly above the 24% achieved by elevating a conventional BF installation.

B. Experimental Setup

The experiment was conducted on the rooftop of the physics building at the Pontifical Catholic University of Peru, Lima, Peru. (12.0714° S, 77.0803° W). The aluminum plates were secured over the designed structure adjacent to both the pyranometers and module as planned on Chapter III.

The final tilt of the reflectors was 25°, measured with a digital level and had a proper extension to the North to account for the sun’s position in the measuring dates. This complete experimental setup is presented as Fig. 22 and Fig. 23.



Fig. 22 East (lateral) view of the arrangement. Circled in red is the module used for testing as well as the pyranometer.



Fig. 23 South (Frontal) view of the arrangement.

C. Results

Ideally, the conditions for the experiment would be to have two systems of non-obstructing solar panels and pyranometers near each other, one with and one without the reflectors. However, due to availability of modules and area in the rooftop, the main goal was to measure a set of sunny and cloudy days with the reflectors installed, and to contrast these data with control days measured without the reflectors.

The logic behind choosing the dates for comparison was twofold: The daily GHI reference yield (Y_r^{GHI}) described in Table III and the similarity among the curves of GHI over time. GHI is not impacted by the implementation of the reflectors and is a good indicator of the total potential irradiance that the

module can capture. Additionally, curve resemblance its helpful in assessing that the GHI over time for each day is similar and comparable to minimize the differences as best as possible.

Pyranometers were used to acquire data related to irradiance, while the installed module recorded its I-V curves, to find the relevant Maximum Power. This implementation had data measured during two distinct weeks. The first week, from the 16th to the 23rd of April, yielded two ideal sunny days (the 18th and 22nd). As mentioned, these days were selected based on Y_r^{GHI} (based on readings on a separated pyranometer facing upwards to the Zenith) measured against a control day with similar total estimated GHI (4th of April) using the same data points before the reflectors were installed. The comparison of GHI between the three days in Fig 24.

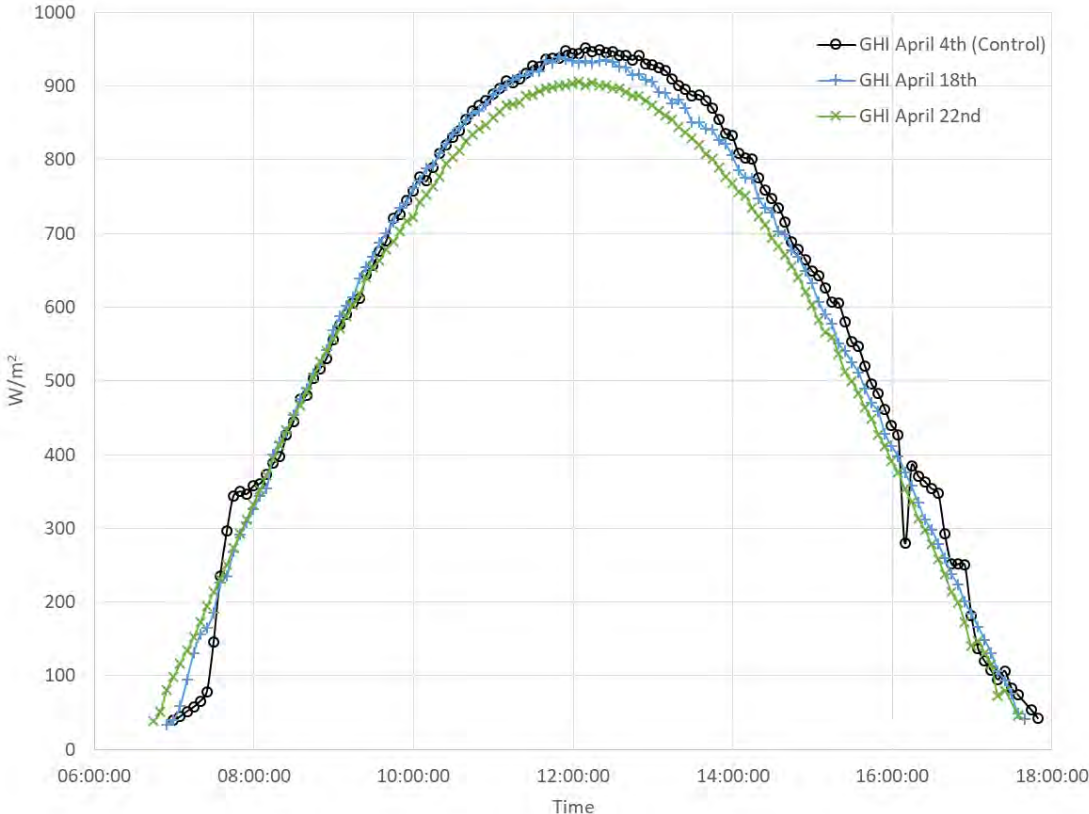


Fig. 24 Global Horizontal Irradiance reading over time for the sunny days.

The second week used for the study was from the 19th to the 26th of June, which yielded two ideal cloudy days (the 19th and 22nd). Using the same methodology as before, the data from these days was measured against another control day with similar Y_r^{GHI} (8th of May), with the same data points before the second reinstallation. Fig 25 presents the same comparison as Fig 24 but for the cloudy days.

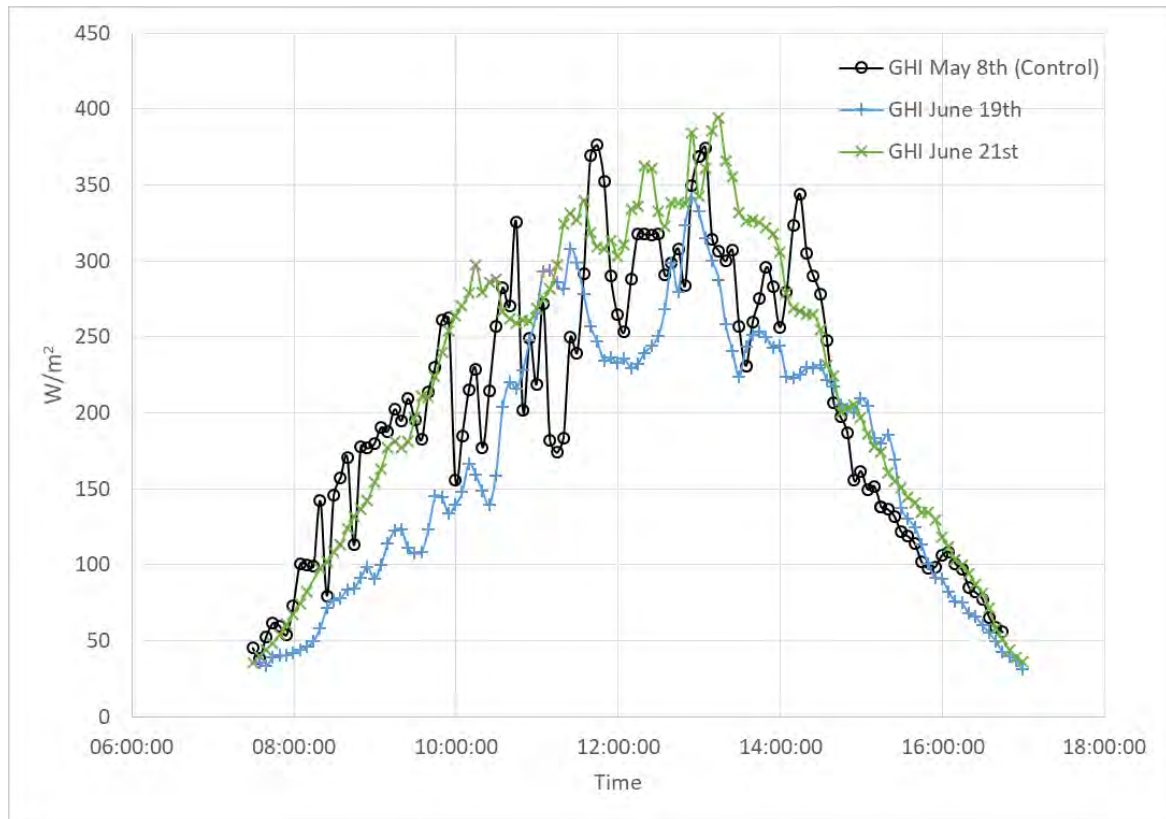


Fig. 255 Global Horizontal Irradiance reading over time for the cloudy days.

Fig. 26 and Fig. 27 demonstrate the irradiance received by the pyranometers facing east and west and their sum for the sunny days, comparing the data with reflectors to the control day without reflectors. Fig. 28 and Fig. 29 do the same for the cloudy days. The sum of the irradiances measured by both pyranometers represents the irradiance received by both sides of the VBF module.

For the sunny days in Fig. 26 and Fig. 27, one can observe the following impacts by the reflectors:

1. At about 9:00, the reflectors start reflecting the direct irradiance towards the pyranometer facing east, enhancing the irradiance it receives.
2. Around 10:00 to 10:30, the irradiance with reflectors measured by the pyranometer facing east reaches its maximum, with a value almost twice as much as without reflectors.
3. Around 14:00 to 14:30, the irradiance with reflectors measured by the pyranometer facing west reaches its maximum, demonstrating a mirror-symmetric behavior as the pyranometer facing east.
4. Compared with the simulated results in Fig. 18, the experimental results are qualitatively similar but yield higher irradiances with reflectors at different times.

One potential reason for this last point may be the limited amount of simulation data. Simulations are run with hourly irradiation information. The experimental result measured irradiance every 5 minutes, resulting in over 120 more data points than the simulation counterpart.

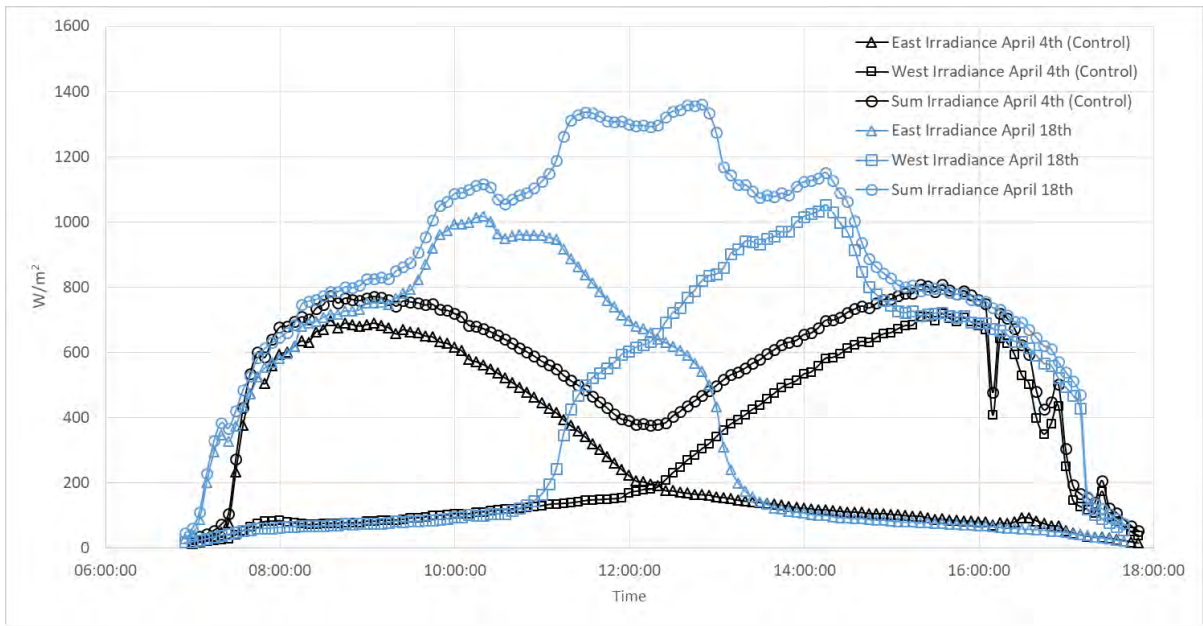


Fig. 26 Irradiance received by the east- and west-facing pyranometers and their sum over time without (black, control) and with reflectors (blue, April 18th).

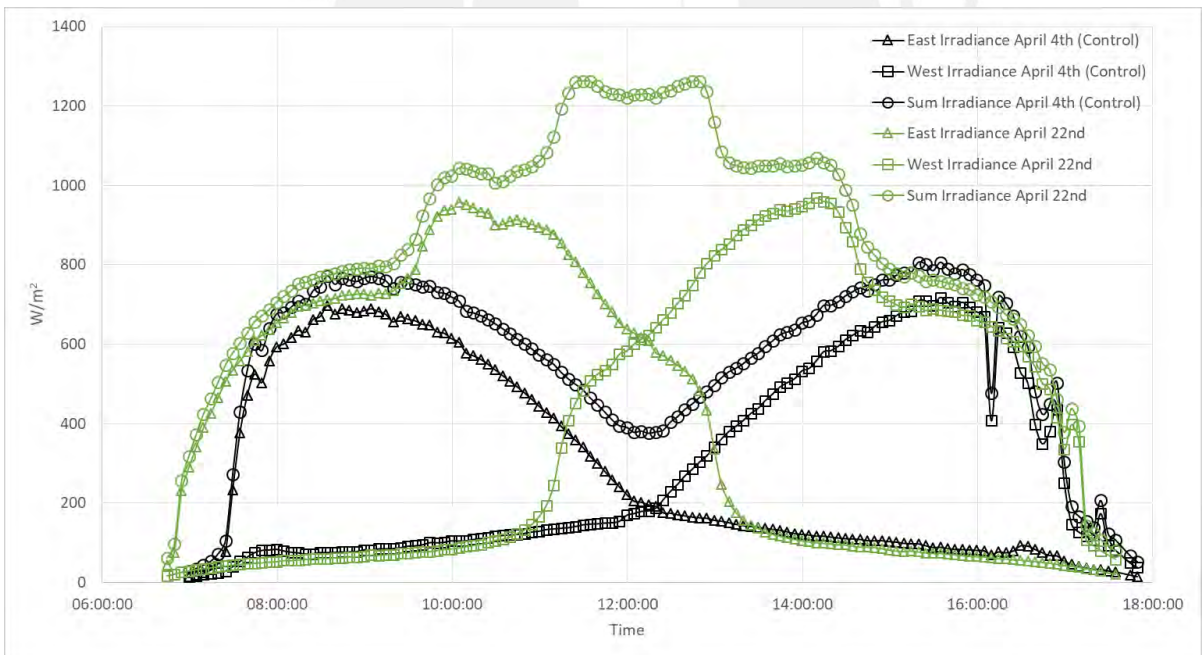


Fig. 27 Irradiance received by the east- and west-facing pyranometers and their sum over time without (black, control) and with reflectors (green, April 22nd).

For the cloudy days in Fig. 28 and Fig. 29, the following can be stated:

1. The difference in the irradiance measured by the east-facing and west-facing pyranometers is negligible, indicating that diffuse irradiance is the dominating component for these cloudy days.

2. Since cloudy conditions on different cloudy days (such as on the control day and the days with reflectors) can differ significantly depending on the type of clouds, estimating the impact by the reflectors requires considering the GHI.

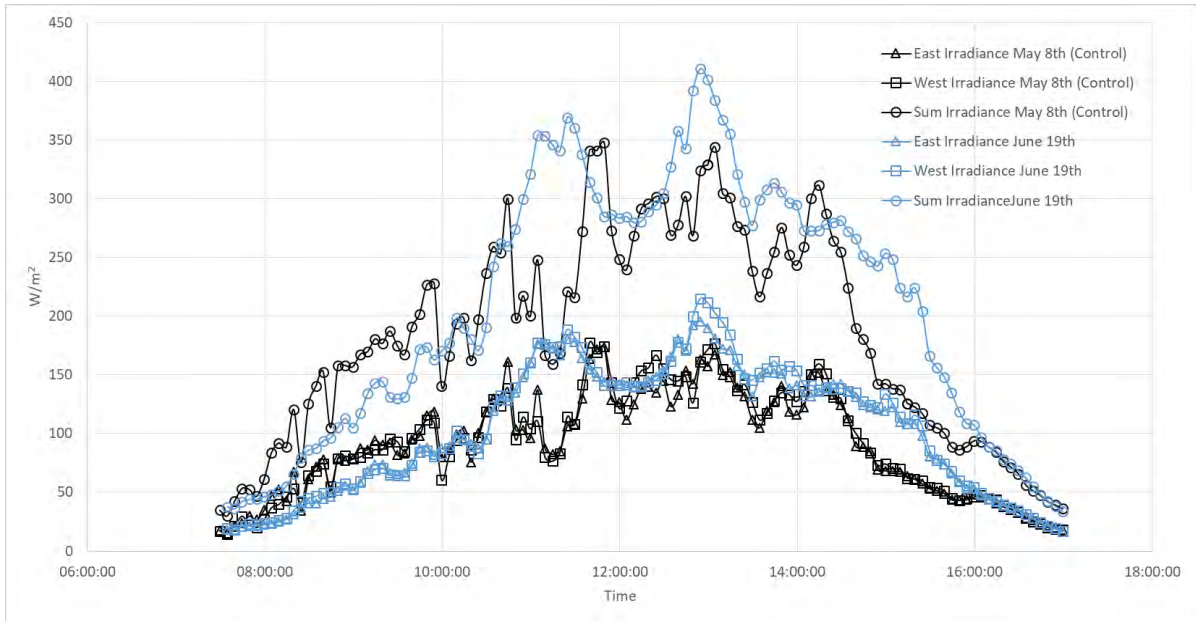


Fig. 28 Irradiance received by the east- and west-facing pyranometers and their sum over time without (black, control) and with reflectors (blue, June 19th).

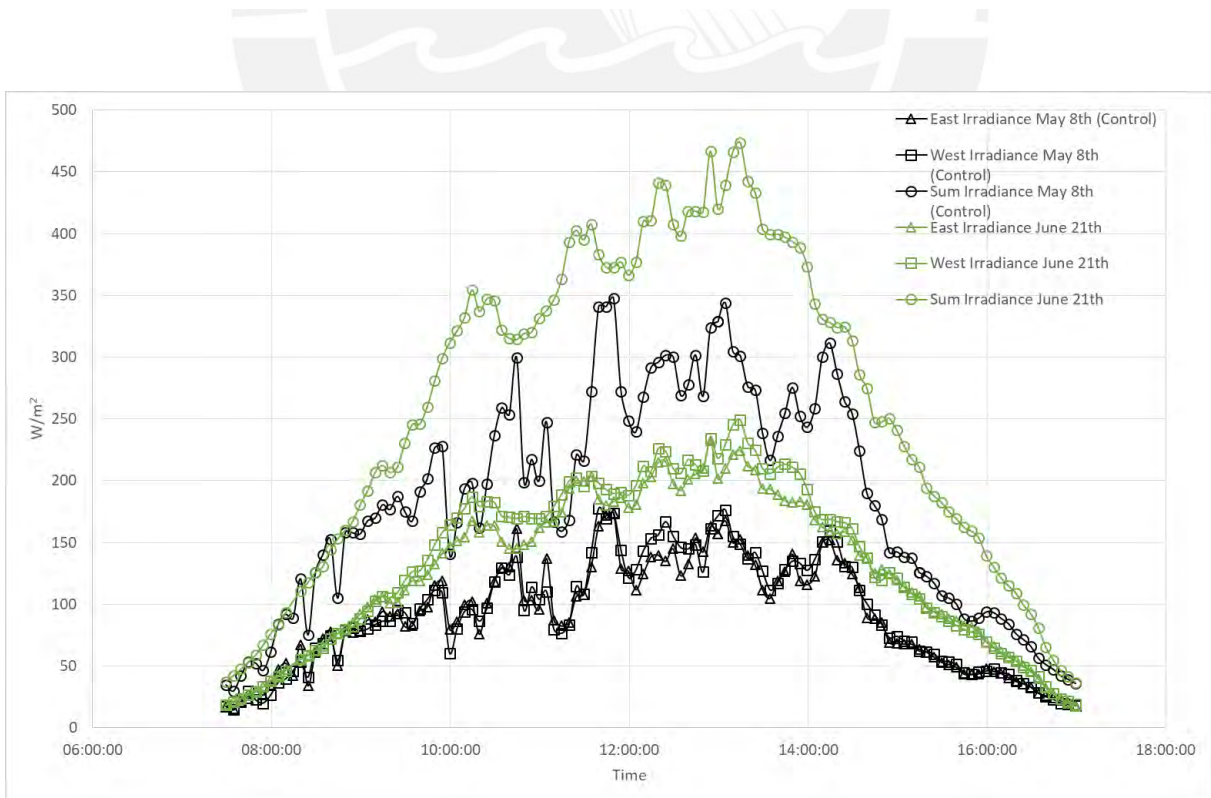


Fig. 29 Irradiance received by the east- and west-facing pyranometers and their sum over time without (black, control) and with reflectors (green, June 21st).

To quantify the impact of the reflectors, Table V and Table VI present the different Yields and the comparative Reflector Gain (Y_r) for each day for sunny and cloudy days, respectively. However, to better account for discrepancies between days there are a few adjustments to calculate the Y_r .

Since clear sky conditions can differ slightly from day to day due to changing atmospheric conditions, these changes can manifest as slightly different irradiances, as can be seen in Fig. 24 and the daily Y_r^{GHI} in Table V for the clear sky days. Therefore, the correction factor $Y_r^{GHI,contr}/Y_r^{GHI,refl}$ is introduced. The reference yields measured by the east and west-facing pyranometers, Y_r^E and Y_r^W , respectively, show similar values, confirming the symmetry of the irradiance evolution in Fig. 27. Their sum Y_r^{E+W} is smaller than Y_r^{GHI} for the control day without reflectors, as seen by the ratio Y_r^{E+W}/Y_r^{GHI} of 0.93. With reflectors, we observe an enhancement by a factor of 1.48 for both days. By calculating the ratio $Y_r^{E+W,refl}/Y_r^{E+W,contr}$, we quantify the impact of the reflectors on Y_r^{E+W} with respect to the control day without reflectors. Multiplying this ratio by the correction factor $Y_r^{GHI,contr}/Y_r^{GHI,refl}$ gives the *Reflector Y_r Gain*, which for both days is 1.59. This factor indicates that the reflectors enhance the irradiation reaching the east- and west-facing pyranometers throughout the day by 59 %.

TABLE V
GHI Reference Yield, East Reference Yield, West Reference Yield and Module Reference Yield and Respective Reflector Gain for Each of the Sunny Days Without (Control) and With Reflectors

Day	Y_r^{GHI} (kWh/kW)	$\frac{Y_r^{GHI,contr}}{Y_r^{GHI,refl}}$	Y_r^E (kWh/kW)	Y_r^W (kWh/kW)	Y_r^{E+W} (kWh/kW)	$\frac{Y_r^{E+W}}{Y_r^{GHI}}$	$\frac{Y_r^{E+W,refl}}{Y_r^{E+W,contr}}$	Reflector Y_r Gain
April 4 th (control)	6.57	-	3.07	3.04	6.11	0.93	-	-
April 18 th	6.46	1.02	4.74	4.80	9.54	1.48	1.56	1.59
April 22 nd	6.25	1.05	4.70	4.53	9.23	1.48	1.51	1.59

TABLE VI
GHI Reference Yield, East Reference Yield, West Reference Yield and Module Reference Yield and Respective Reflector Gain for Each of the Cloudy Days Without (Control) and With Reflectors

Day	Y_r^{GHI} (kWh/kW)	$\frac{Y_r^{GHI,contr}}{Y_r^{GHI,refl}}$	Y_r^E (kWh/kW)	Y_r^W (kWh/kW)	Y_r^{E+W} (kWh/kW)	$\frac{Y_r^{E+W}}{Y_r^{GHI}}$	$\frac{Y_r^{E+W,refl}}{Y_r^{E+W,contr}}$	Reflector Y_r Gain
May 8 th (control)	1.91	-	0.87	0.88	1.75	0.92	-	-
June 19 th	1.62	1.18	0.97	0.99	1.96	1.21	1.12	1.32
June 21 st	2.07	0.92	1.21	1.28	2.49	1.20	1.42	1.31

In Table VI, the correction factors for the cloudy days show a more significant variation of Y_r^{GHI} between the three days due to the more considerable variability of the atmospheric conditions and clouds during cloudy days. Following the same procedure as before demonstrates that for cloudy days, the reflectors enhance the irradiation reaching the east- and west-facing pyranometers throughout the day by about 32 %.

Next, the traced I-V curves of the VBF module for the same days were analyzed. Fig. 30 presents the IV curves at different measurements in time for the summer control day (April 4th). It is important to note that the data points were separated into two graphics. The first one (Fig. 30(a)) draws the values from the early morning until 12:00 pm, and the second one (Fig. 30(b)) from 12:00 pm onwards. As presented in the figures, there are step-like artifacts in the IV curve measurements throughout the day, which are most pronounced in the morning to noon, when the direct irradiance of the sun illuminates the east-facing back side of the module. In Fig. 30(a), one can observe current steps in the I-V curve in two voltage ranges, one around 11 V and another around 22 V. These current steps are an indication of the activation of the bypass diodes in the module, which are caused most likely by partial shadowing due to the frame in the backside. These steps become more pronounced when the impact of partial shadowing is expected to be highest, i.e., when the partial shadow covers close to half the area of the backside of the module from around 10:00 am to 11:00 am. The steps become least pronounced when the partial shadow coverage is lowest very early in the morning at the lowest sun elevation or when it fully covers the backside near noon when the sun is at its highest elevation. In Fig. 30(b), the direct irradiance illuminates the west-facing front side of the module, where no partial frame shadowing is cast on the illuminated area due to the module design. Still, some minor steps can be observed in the I-V curves, which most likely originate from the partial shadowing by the frame on the backside for the diffuse and reflected irradiance.

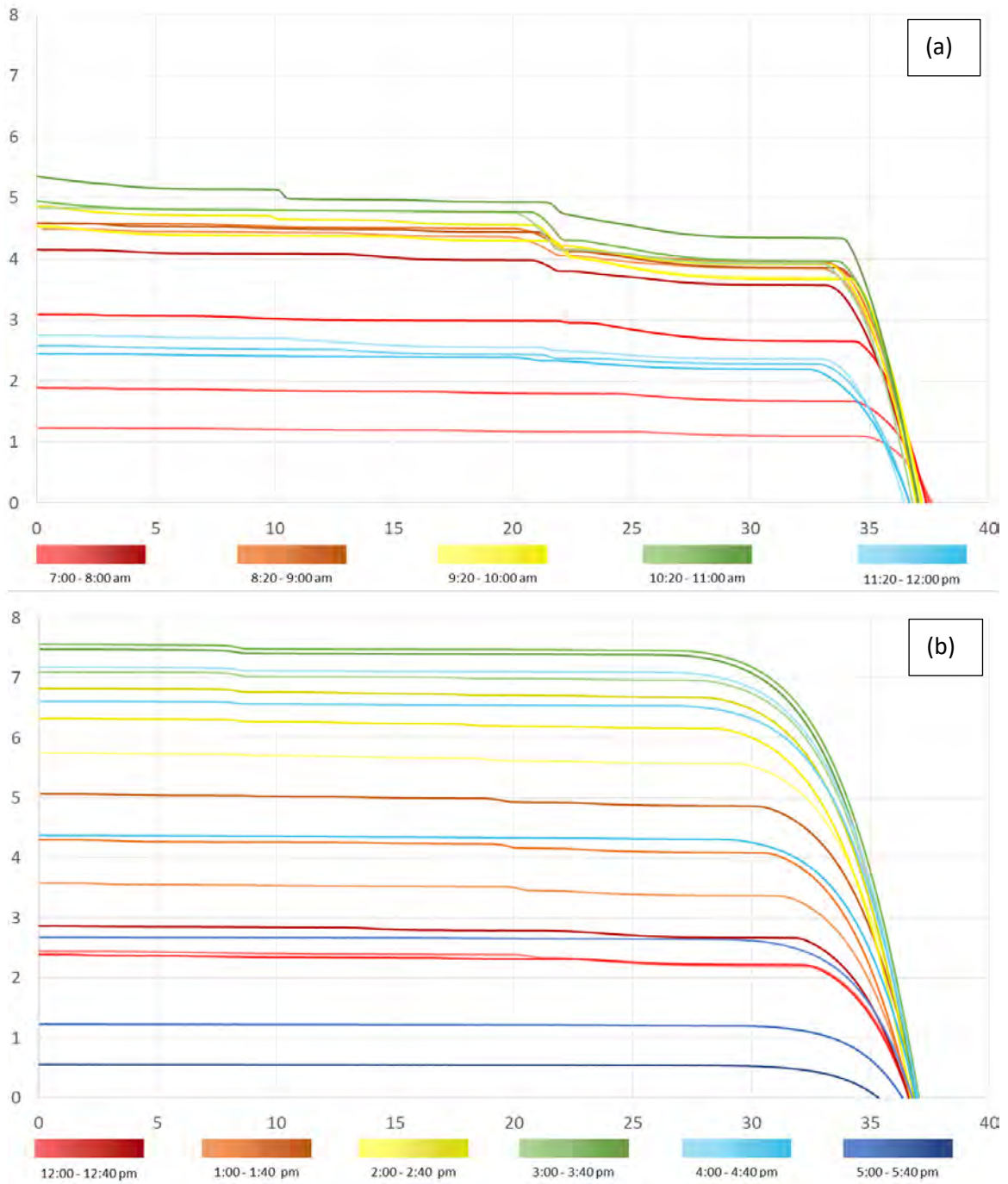


Fig. 30 I-V Curves for the Sunny Control Day. (a) hours between 7 a.m. to 12 m. (b) hours from 12 m. to 5:40 p.m.

From the measured I-V curves, the power at the maximum power point was extracted and plotted over time in Fig. 31 and 32 for the clear and cloudy sky days, respectively. When compared to the sum of the irradiances received by the east- and west-facing pyranometers in Fig. 26 and 27, the evolution of the maximum power in Fig. 31 is asymmetric, with power values before solar noon being lower than in the afternoon. Before the solar noon, the backside of the module receives the direct irradiance of the sun, and in the afternoon, the front receives it. Therefore, this asymmetry originates predominantly from the power bifaciality of the VBF module, with the backside facing east having a power conversion efficiency (73 ± 5) % of the front side facing west. The partial shadowing on the backside illumination by the frame, observed in the I-V curves in Fig. 30(a), probably also contributes to the lower power values before noon. Comparing the power for the control day without reflectors with the power of both days with reflectors, a power enhancement is evident starting around 9:00 and ending around 15:30, similarly to the irradiance enhancement observed in Fig. 26 and 27.

In Fig. 32, no asymmetry in power is evident for the cloudy days, as the diffuse irradiance is the dominating component, and thus, both sides of the module receive similar irradiance throughout the day, as shown in Fig. 28 and 29.

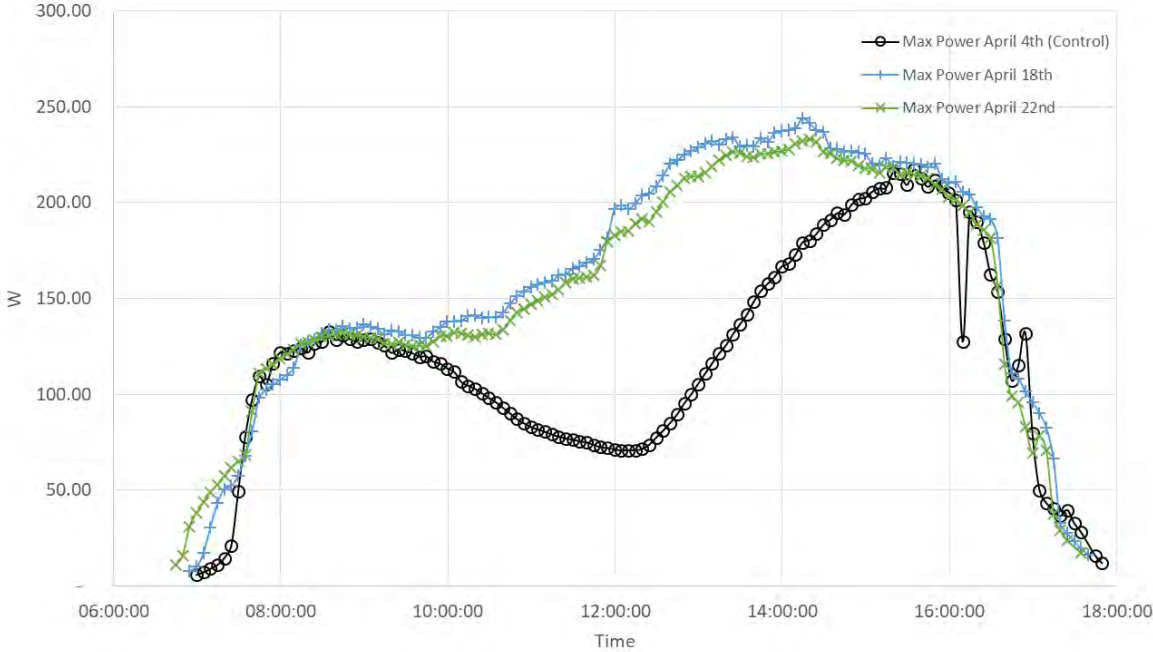


Fig. 31 Maximum power over time comparison for sunny days.

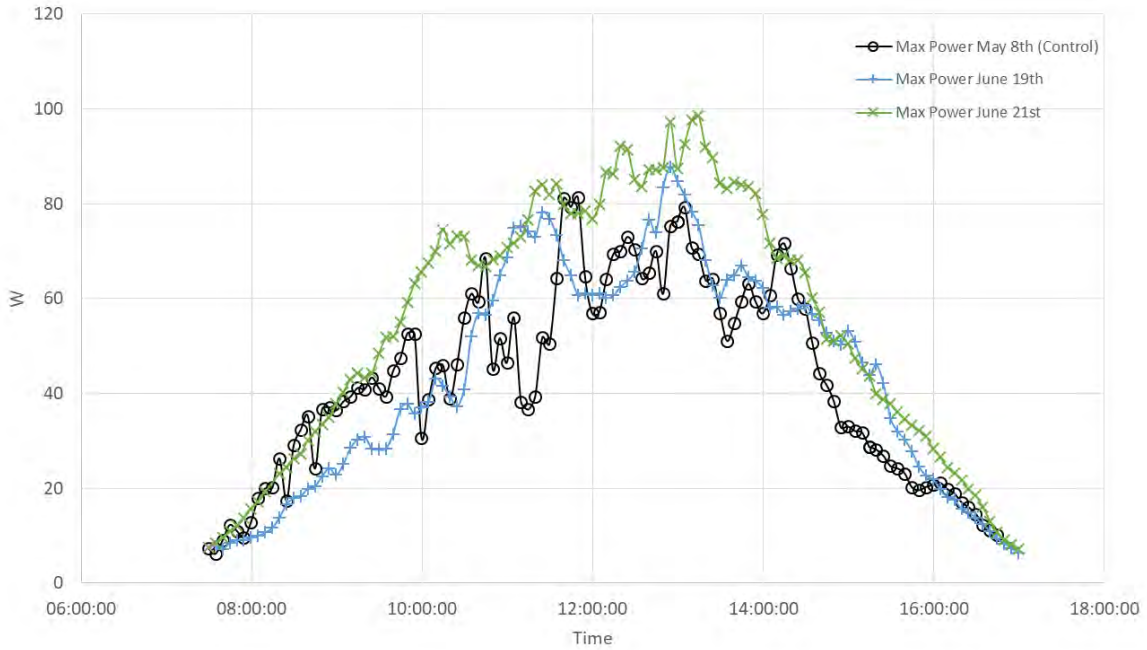


Fig. 32 Maximum power over time comparison for cloudy days.

Table VII and Table VIII, for sunny and cloudy days, respectively, present the Array Yield Y_p in terms of power conversion and the Gain in relation to the control for both days with reflectors. Array Yield was calculated by dividing the module's daily integrated maximum power by its nominal power output at STC. To compensate for the different GHI between the three cloudy days, the correction factor $Y_r^{GHI,contr} / Y_r^{GHI,refl}$ is used to calculate the Reflector Y_p Gain. In Table VII, for the sunny days, the Reflector Y_p Gain is 1.39 and 1.38, indicating that the reflectors lead to an enhancement of up to 39 % in the total power throughout the day. The enhancement in integrated power (39 %) is lower than the enhancement in integrated irradiance (59 %), possibly due to the power bifaciality (73±5) %, which reduces the power conversion efficiency when the back side of the VBF modules is irradiated in the morning by the direct irradiance and throughout the day by the diffuse irradiance.

TABLE VII
Module's Array Yield and Gain in Sunny Days.

Day	$Y_p (kWh/kW)$	$\frac{Y_r^{GHI,contr}}{Y_r^{GHI,refl}}$	Reflector Y_p Gain
April 4 th (control)	3.98	-	-
April 18 th	5.41	1.02	1.39
April 22 nd	5.22	1.05	1.38

In Table VIII, for the cloudy days, the *Reflector Y_p Gain* is to 1.22 and 1.19, indicating that the reflectors lead to an enhancement of up to 22 % in the total power throughout the day, which is also lower than the enhancement in the integrated irradiance of up to 32 %.

Interestingly, the ratio of the integrated power and irradiance enhancements 22 %/32 % for the cloudy days and the ratio 39 % / 59 % for the sunny days are very similar, approximating $\sim 2/3$, which falls within the range of the power bifaciality (73±5) %, also considering some minor loss due to partial shadowing on the backside by the frame.

TABLE VIII
Module's Array Yield and Gain in Cloudy Days.

<i>Day</i>	$Y_p(kWh/kW)$	$\frac{Y_r^{GHI,contr}}{Y_r^{GHI,refl}}$	<i>Reflector Y_p Gain</i>
May 8 th (control)	1.26	-	-
June 19 th	1.30	1.18	1.22
June 21 st	1.63	0.92	1.19

Finally, Table IX summarizes the previously commented results, with the added Module Performance Ratio.

TABLE IX
Comparison Table with 2 Distinct Module Performance Ratios, by Comparing Array Yield to the GHI Reference Yield and the Module Reference Yield Separately.

<i>Day</i>	$Y_r^{GHI} (kWh/kW)$	$Y_r^{E+W} (kWh/kW)$	$Y_p (kWh/kW)$	PR^{GHI}	PR^{E+W}
April 4th (Control)	6.57	6.11	3.98	0.61	0.65
April 18th	6.46	9.54	5.41	0.84	0.57
April 22nd	6.25	9.23	5.22	0.83	0.57
May 8th (Control)	1.91	1.75	1.26	0.66	0.72
June 19th	1.62	1.96	1.30	0.80	0.66
June 21st	2.07	2.49	1.63	0.79	0.65

As evidenced in the Table, the GHI performance ratio was sustainably higher on both sunny and cloudy days compared to their respective controls. While the Module Performance Ratio was lower compared to the control, this is because the latter uses as a denominator the Module Reference Yield, which is already accounting for the additional irradiance received in the pyranometers due to the reflectors. This difference then can be explained by the inefficiency in converting all the additional irradiance into actual power.

VII. CONCLUSIONS

The yield and performance enhancement of vertical bifacial (VBF) modules using fixed aluminum reflectors was demonstrated. The irradiance perceived by the pyranometer and the maximum power traced by the module using the I-V curves were remarkably enhanced by the reflected irradiation from the plates on typical sunny days and improved on cloudy days. As such, the key conclusions of this research are the following:

- The simulation estimated a Module Reference Yield (kWh/kW/day) of 8.26 for the sunny days and 2.75 for the cloudy days with the reflectors installed. The experimental average for these values was 9.39 and 2.23 for sunny and cloudy days respectively. This means that the simulation undershot the gain for sunny days and overshot the same metric for the cloudy days. However, the input variables from the simulation differ from those on the experiment (GHI, DNI, DHI), as such the results are not comparable per se, but were used more as an indicator for the optimal reflector tilt
- Compared to the distinct control day without reflectors, the pyranometer perceived an average of 59% more irradiation during ideal sunny days and 32% during ideal cloudy days in the weeks where the reflector was installed when controlling for the difference in GHI. While this proved itself successful on its own, it should be noted that the gain in cloudy days presented a great amount of variability between both measurements before adjusting for the difference in GHI, so the installation for this type of cloud conditions should be further explored.
- There was a substantial average increment of 39% in the maximum power output for ideal sunny days and 21% during ideal cloudy days compared to the VBF during the control days.
- The research helped demonstrate that east-west oriented VBF systems with fixed reflectors on both the front and rear ends (rVBFs) properly enhance the power generation of this type of roof top PV systems. This opens the discussion for this type of implementation on a larger scale, to determine the feasibility of this study's design.
- The implemented reflectors are directly appended to the VBF system, which means that once the sun has an elevation lower than 25° in the sky it will start to project shadows on the module, while the proposed system still achieved a significant yield, the spacing or elevation between the reflectors and the module is another variable that can be considered when contemplating a larger scale implementation or building applied photovoltaics (BAPV).
- While directly reflecting aluminum was chosen for the present experiment after a great deal of testing, there may be other factors that could be considered to select an even better material. One of these could be using the External Quantum Efficiency (EQE). The EQE of a module restricts the number of electrons that can be obtained from incident photons relative to their wavelength. This could a more thorough way to assess potential reflector materials, compared to only using the Spectral Solar Irradiance, focusing even more precisely on which wavelengths the module can

actually act upon. Additionally, further tests could be performed using more diffusing types of reflectors, to analyze experimentally which type of reflectivity (specular or diffuse) is more optimal for enhancing VBFs.



REFERENCES

- [1] J. Eguren, F. Martínez-Moreno, P. Merodio, and E. Lorenzo, "First bifacial PV modules early 1983," *Solar Energy*, vol. 243, pp. 327–335, Sep. 2022, doi: 10.1016/j.solener.2022.08.002. Available: <https://doi.org/10.1016/j.solener.2022.08.002>
- [2] International Technology Roadmap for Photovoltaic, "International Technology Roadmap for Photovoltaic," Verband Deutscher Maschinen- und Anlagenbau (VDMA), 12, Apr. 2023.
- [3] S. Bhaduri and A. Kottantharayil, "Mitigation of Soiling by Vertical Mounting of Bifacial Modules," *IEEE Journal of Photovoltaics*, vol. 9, no. 1, pp. 240–244, 2019, doi: 10.1109/jphotov.2018.2872555
- [4] G. P. Smestad et al., "Modelling photovoltaic soiling losses through optical characterization," *Scientific Reports*, vol. 10, no. 1, 2020, doi: 10.1038/s41598-019-56868-z
- [5] E. Cabrera et al., ATAMOS TEC Project: Soiling impact on bifacial modules with different mounting geometry in the Atacama desert in Chile. 2018. doi: 10.1109/pvsc.2018.8547697. Available: <https://doi.org/10.1109/pvsc.2018.8547697>
- [6] M. Riaz, H. Imran, R. Younas, M. A. Alam, and N. Z. Butt, "Module technology for Agrivoltaics: Vertical bifacial versus tilted monofacial farms," *IEEE Journal of Photovoltaics*, vol. 11, no. 2, pp. 469–477, Mar. 2021, doi: 10.1109/jphotov.2020.3048225. Available: <https://doi.org/10.1109/jphotov.2020.3048225>
- [7] P. E. Campana, B. Stridh, S. Amaducci, and M. Colauzzi, "Optimisation of vertically mounted agrivoltaic systems," *Journal of Cleaner Production*, vol. 325, p. 129091, Nov. 2021, doi: 10.1016/j.jclepro.2021.129091. Available: <https://doi.org/10.1016/j.jclepro.2021.129091>
- [8] B. Willockx, C. Lavaert, and J. Cappelle, "Performance evaluation of vertical bifacial and single-axis tracked agrivoltaic systems on arable land," *Renewable Energy*, vol. 217, p. 119181, Nov. 2023, doi: 10.1016/j.renene.2023.119181. Available: <https://doi.org/10.1016/j.renene.2023.119181>
- [9] M. R. Khan, A. Hanna, X. Sun, and M. A. Alam, "Vertical bifacial solar farms: Physics, design, and global optimization," *Applied Energy*, vol. 206, pp. 240–248, 2017, doi: 10.1016/j.apenergy.2017.08.042
- [10] X. Sun, M. R. Khan, C. Deline, and M. A. Alam, "Optimization and performance of bifacial solar modules: A global perspective," *Applied Energy*, vol. 212, pp. 1601–1610, 2018, doi: 10.1016/j.apenergy.2017.12.041

- [11] U. A. Yusufoglu et al., "Simulation of Energy Production by Bifacial Modules with Revision of Ground Reflection," *Energy Procedia*, vol. 55, pp. 389–395, 2014, doi: 10.1016/j.egypro.2014.08.111
- [12] B. Durusoy, T. Ozden, and B. G. Akinoglu, "Solar irradiation on the rear surface of bifacial solar modules: a modeling approach," *Scientific Reports*, vol. 10, no. 1, 2020, doi: 10.1038/s41598-020-70235-3
- [13] J. Johnson and S. Manikandan, "Rear Side Solar Radiation Model of Bifacial Photovoltaic Module for Equatorial zone," *IOP Conference Series: Materials Science and Engineering*, vol. 1130, no. 1, p. 012018, 2021, doi: 10.1088/1757-899x/1130/1/012018
- [14] V. Muthu and G. Ramadas, "Experimental Investigation of 4E Performance of A Vertical Bifacial Solar Module During Summer and Winter," *Experimental Investigation of 4E Performance of a Vertical Bifacial Solar Module During Summer and Winter*, 2021, doi: 10.21203/rs.3.rs-711055/v1
- [15] P. K. Sahu, J. N. Roy, C. Chakraborty, and S. Sundaram, "A New Model for Estimation of Energy Extraction from Bifacial Photovoltaic Modules," *Energies*, vol. 14, no. 16, p. 5089, 2021, doi: 10.3390/en14165089
- [16] S. Pal and R. Saive, "Output Enhancement of Bifacial Solar Modules Under Diffuse and Specular Albedo," *2021 IEEE 48th Photovoltaic Specialists Conference (PVSC)*, 2021, doi: 10.1109/pvsc43889.2021.9519093
- [17] T. C. R. Russell, R. Saive, A. Augusto, S. G. Bowden, and H. A. Atwater, "The Influence of Spectral Albedo on Bifacial Solar Cells: A Theoretical and Experimental Study," *IEEE Journal of Photovoltaics*, vol. 7, no. 6, pp. 1611–1618, 2017, doi: 10.1109/jphotov.2017.2756068
- [18] N. Riedel et al., "The effect of spectral albedo in bifacial photovoltaic performance," *Solar Energy*, vol. 231, pp. 921–935, Jan. 2022, doi: 10.1016/j.solener.2021.12.023. Available: <https://doi.org/10.1016/j.solener.2021.12.023>
- [19] M. R. Khan, E. Sakr, X. Sun, P. Bermel, and M. A. Alam, "Ground sculpting to enhance energy yield of vertical bifacial solar farms," *Applied Energy*, vol. 241, pp. 592–598, 2019, doi: 10.1016/j.apenergy.2019.01.168
- [20] M. A. Zahid, H. Yousuf, Y. Kim, J. Yi, and S. K. Dhungel, "A novel approach for power enhancement of vertical mounted bifacial photovoltaic system using reflecting mirrors," *Journal of Cleaner Production*, vol. 397, p. 136541, Feb. 2023, doi: 10.1016/j.jclepro.2023.136541. Available: <https://doi.org/10.1016/j.jclepro.2023.136541>
- [21] J. L. Cardoso, A. Mutuberria, C. Marakkos, P. Schoettl, T. Osório, and I. Les, "New functionalities for the Tonatiuh ray-tracing software. 2018. doi: 10.1063/1.5067212. Available: <https://doi.org/10.1063/1.5067212>

- [22] S. A. Pelaez and C. Deline, “bifacial_radiance: a python package for modeling bifacial solar photovoltaic systems,” *Journal of Open Source Software*, vol. 5, no. 50, p. 1865, Jun. 2020, doi: 10.21105/joss.01865. Available: <https://doi.org/10.21105/joss.01865>
- [23] E. Maxwell, T. Stoffel, and R. E. Bird, “Measuring and modeling solar irradiance on vertical surfaces,” Jul. 1986. doi: 10.2172/5439042. Available: <https://doi.org/10.2172/5439042>
- [24] Gh. Kamali, I. Moradi, and A. Khalili, “Estimating solar radiation on tilted surfaces with various orientations: a study case in Karaj (Iran),” *Theoretical and Applied Climatology*, vol. 84, no. 4, pp. 235–241, Sep. 2005, doi: 10.1007/s00704-005-0171-y. Available: <https://doi.org/10.1007/s00704-005-0171-y>
- [25] R. J. Koschel, *Illumination Engineering*. 2013. doi: 10.1002/9781118462539. Available: <https://doi.org/10.1002/9781118462539>
- [26] J. J. O’Gallagher, *Nonimaging optics in solar energy*. 2008. doi: 10.1007/978-3-031-79420-9. Available: <https://doi.org/10.1007/978-3-031-79420-9>
- [27] I. S. Nefedov, L. A. Melnikov, and E. Nefedov, *Asymmetrical hyperbolic media and their potential applications in photovoltaics and photonics*. 2013. doi: 10.1117/12.2017607. Available: <https://doi.org/10.1117/12.2017607>
- [28] A. Ustaoglu, U. Ozbey, and H. Torlaklı, “Numerical investigation of concentrating photovoltaic/thermal (CPV/T) system using compound hyperbolic –trumpet, V-trough and compound parabolic concentrators,” *Renewable Energy*, vol. 152, pp. 1192–1208, Jun. 2020, doi: 10.1016/j.renene.2020.01.094. Available: <https://doi.org/10.1016/j.renene.2020.01.094>
- [29] A. Ustaoglu, V. Akgül, and J. Okajima, “Performance investigation of truncated low concentrating photovoltaic-thermal systems with V-trough, compound hyperbolic and compound parabolic concentrators,” *Applied Thermal Engineering*, vol. 232, p. 121028, Sep. 2023, doi: 10.1016/j.applthermaleng.2023.121028. Available: <https://doi.org/10.1016/j.applthermaleng.2023.121028>
- [30] Amusan and Otokunefor, “The Effect of Shadow on the Output Performance of Solar Module,” *Conference Proceedings on National Conference on Energy and Environment Organized by Switch Tech Mega Solutions Ltd at National Center for Energy and Environment*, Dec. 2016.
- [31] A. Díaz-Rubio, V. Asadchy, A. Elsakka, and S. A. Tretyakov, “From the generalized reflection law to the realization of perfect anomalous reflectors,” *Science Advances*, vol. 3, no. 8, Aug. 2017, doi: 10.1126/sciadv.1602714. Available: <https://doi.org/10.1126/sciadv.1602714>

- [32] J.-Y. Choi, B. Y. Choi, J.-E. Kim, S.-T. Ryu, C. T. Rim, and Y.-S. Kim, "New curved reflectors for significantly enhanced solar power generation in four seasons," *Energies*, vol. 12, no. 23, p. 4602, Dec. 2019, doi: 10.3390/en12234602. Available: <https://doi.org/10.3390/en12234602>
- [33] P. Ooshaksaraei, K. Sopian, R. Zulkifli, M. A. Alghoul, and S. H. Zaidi, "Characterization of a bifacial photovoltaic panel integrated with external diffuse and semimirror type reflectors," *International Journal of Photoenergy*, vol. 2013, pp. 1–7, Jan. 2013, doi: 10.1155/2013/465837. Available: <https://doi.org/10.1155/2013/465837>
- [34] H. Wu, A. Emadi, G. De Graaf, J. Leijtens, and R. F. Wolffenbuttel, "Design and fabrication of an Albedo Insensitive analog Sun sensor," *Procedia Engineering*, vol. 25, pp. 527–530, Jan. 2011, doi: 10.1016/j.proeng.2011.12.131. Available: <https://doi.org/10.1016/j.proeng.2011.12.131>
- [35] "Reference Air Mass 1.5 Spectra," *Grid Modernization | NREL*. Available: <https://www.nrel.gov/grid/solar-resource/spectra-am1.5.html>
- [36] "Weather Data by Location," <https://energyplus.net/>. Available: https://energyplus.net/weather-location/south_america_wmo_region_3/PER/PER_Lima.846280_IWEC. [Accessed: Nov. 15, 2022]

